Dalton Transactions

Cite this: *Dalton Trans.*, 2012, **41**, 9349

www.rsc.org/dalton

PAPER

Tin(II) amide/alkoxide coordination compounds for production of Sn-based nanowires for lithium ion battery anode materials†

Timothy J. Boyle,*[a] Thu Q. Doan,[a] Leigh Anna M. Steele,[a] Christopher Apblett,[a] Sarah M. Hoppe,[a] Krista Hawthorne,[a] Robin M. Kalinich[a] and Wolfgang M. Sigmund[b,c]

Received 16th January 2012, Accepted 13th May 2012
DOI: 10.1039/c2dt30772c

A series of tin(II) amide alkoxides ($[(OR)Sn(NMe_2)]_n$) and tin(II) alkoxides ($[Sn(OR)_2]_n$) were investigated as precursors for the production of tin oxide (SnO_x) nanowires. The precursors were synthesized from the metathesis of tin dimethylamide ($[Sn(NMe_2)_2]_2$) and a series of aryl alcohols {H-OAr = H-$OC_6H_4(R)$-2: R = CH_3 (H-*o*MP), $CH(CH_3)_2$ (H-*o*PP), $C(CH_3)_3$ (H-*o*BP)] or [H-$OC_6H_3(R)_2$-2,6: R = CH_3 (H-DMP), $CH(CH_3)_2$ (H-DIP), $C(CH_3)_3$ (H-DBP)]}. The 1 : 1 products were all identified as the dinuclear species $[(OAr)Sn(\mu\text{-}NMe_2)]_2$ where OAr = *o*MP (**1**), *o*PP (**2**), *o*BP (**3**), DMP (**4**), DIP (**5**), DBP (**6**). The 1 : 2 products were identified as either a polymer ($[Sn(\mu\text{-}OAr)_2]_\infty$ (where OAr = *o*MP (**7**), *o*PP (**8**)), dinuclear $[(OAr)Sn(\mu\text{-}OAr)]_2$ (where OAr = *o*BP (**9**), DMP (**10**) or DIP/$HNMe_2$ (**11**)), or mononuclear $[Sn(DBP)_2]$ (**12**) complexes. These novel families of compounds (heteroleptic **1–6**, and homoleptic **7–12**) were evaluated for the production of SnO_x nanowires using solution precipitation (SPPT; oleylamine/octadecene solvent system) or electrospinning (ES; THF solvent) processing conditions. The SPPT route that employed the heteroleptic precursors yielded mixed phases of Sn^o : romarchite [**1** (100 : 0); **2** (80 : 20); **3** (68 : 32); **4** (86 : 14); **5** (66 : 35); **6** (88 : 12)], with a variety of spherical sized particles [**1** (350–900 nm); **2** (150–1200 nm); **3** (250–950 nm); **4** (20–180 nm); **5** (80–400 nm); **6** (40–200 nm)]. For the homoleptic precursors, similar phased [**7** (80 : 20); **8** (23 : 77); **9** (15 : 85); **10** (34 : 66); **11** (77 : 23); **12** (77 : 23)] spherical nanodots were isolated [**7** (50–300 nm); **8**: (irregular); **10** (200–800 nm); **11** (50–150 nm); **12** (50–450 nm)], except for **9** which formed polycrystalline rods [Sn^o : romarchite (15 : 85)] with aspect ratios >100. From ES routes, the heteroleptic species were found to form 'tadpole-shaped' materials whereas the homoleptic species formed electrosprayed nanodots. The one exception noted was for **7**, where, without use of a polymer matrix, nanowires of Sn^o, decorated with micron sized 'balls' were observed. Due to the small amount of material generated, PXRD patterns were inconclusive to the identity of the generated material; however, cyclic voltammetry on select samples was used to tentatively identify the final Sn^o (from **7**) with the other sample identified as SnO_x (from **1**).

Introduction

Due to their expected high energy density, reasonable cycle life, long storage times, and 'green' status, lithium ion battery (LIB) power sources are of interest for meeting the consumer's demand for cheaper, smaller, and safer but more powerful devices. However, several drawbacks limit the widespread growth of LIB technology, such as the need for higher energy capacity, longer cycle life, and faster recharging rates. In particular, the strain the anode and cathode materials undergo during the cycling of Li ions can cause significant mechanical failures.[1–7] For example, upon Li ion cycling of Si^o (one of the most attractive LIB anode materials)[1,2] undergoes a more than 400% volume change, which destroys the crystalline material. Recently, a report by Cui and coworkers demonstrated that Si^o nanowires can survive this cycling strain while maintaining high capacities (>3500 mAh g^{-1} for 20 cycles).[3] However, several drawbacks were noted for this system such as irreversible capacity losses, laborious preparative routes, and limitations to large-scale production.

Alternatively, tin oxide (SnO_x) has attracted increasing interest as use as a LIB anode material due to the theoretical value of 990 mAh g^{-1} expected from the oft-cited $Li_{4.4}Sn$.[4–7] Unfortunately, the formation of this alloy also undergoes a volume

---

[a] *Sandia National Laboratories, Advanced Materials Laboratory, 1001 University Boulevard SE, Albuquerque, New Mexico, 87106, USA. E-mail: tjboyle@Sandia.gov; Fax: +1 (505)272-7336; Tel: +1 (505)272-7625*
[b] *Department of Materials Science and Engineering, University of Florida, Gainesville, Florida 32611-6400, USA*
[c] *WCU Department of Energy Engineering, Hanyang University, Seoul, South Korea*

† Electronic supplementary information (ESI) available: Structure plots of all compounds (**1–12** and **S1–S3**), and the quantitative analyses of the PXRD of the generated Sn^o/SnO (17 pages). CCDC 843197–843202, 843204–843212. For ESI and crystallographic data in CIF or other electronic format see DOI: 10.1039/c2dt30772c

expansion (300%), which 'pulverizes' the material.[7] As noted for the Si^o system, Lee and Wang have reported SnO_x nanowires possess a capacity of ~1100 mAh g^{-1}, however, significant morphological changes were noted upon cycling.[8] Since this is higher than the theoretical capacity of SnO_2, we became interested in generating SnO_x nanowires and exploring their utility as anodes for LIB applications. Previous routes for the production of SnO_x nanowires for LIBs utilized a vapor–liquid–solid (VLS) mechanism from the thermal evaporation,[9,10] hard templating,[11] or salt melts.[12] Recently, a report by Tatte *et al.*[13] was disseminated that employs a true sol–gel processing approach by a 'direct pull' process of metal *tert*-butoxide $[M(OBu^t)_y]$ oils exposed to water to generate MO_x (M = Sn, Ti, Zr, Hf, and Ce) nanowires with an aspect ratio of up to 10 000. These routes are complicated and/or expensive setups that not necessarily amenable to large scale production.

Solution routes to SnO_y nanowires are underexplored but if successful, they will be simple, fast, relatively inexpensive, and amenable to large scale syntheses. For these systems, we favor metal alkoxides ($M(OR)_y$) precursors since they are often commercially available, their physical and chemical properties (*i.e.*, hydrolysis susceptibility, solubility, volatility, *etc.*) can be easily tailored through ligand set manipulations, and they have all the necessary components present (*i.e.*, metal and oxygen) prior to decomposition. The structural arrangement of $M(OR)_y$ (directed by the ligand set employed) has been found to play a role in determining the properties of the final ceramic material produced.[14–24] Often the conversion of $M(OR)_y$ to MO_x is accomplished through hydrolysis by either a one-step polycondensation mechanism, upon exposure to water[2,25] or by an ether elimination[26] (after a series of reaction processes) when organic solvents and water are employed. However, in the processes used in this study, water was omitted to minimize side reactions and the expected oxalate intermediates.[26]

Our previous work[27] with tin(II) amides $[Sn(NMe_2)_2]$ and alkoxides $[Sn(OR)_2]$ led us to investigate the synthesis of tin(II) amide/aryloxides $[Sn(NMe_2)(OAr)]$ and aryloxide $[Sn(OAr)_2]$ for use in the production of nanowires. Following eqn (1) and (2), the dimethyl amide derivative $[Sn(NMe_2)_2]_2$ was independently reacted with a series of aryl alcohols (H-OAr), including $H\text{-}OC_6H_4(R)\text{-}2$: R = CH_3 (H-*o*MP), $CH(CH_3)_2$ (H-*o*PP), $C(CH_3)_3$ (H-*o*BP)] or $[H\text{-}OC_6H_3(R)_2\text{-}2,6$: R = CH_3 (H-DMP), $CH(CH_3)_2$ (H-DIP), $C(CH_3)_3$ (H-DBP)]. The products were all identified as the dinuclear species for the heteroleptic compounds (eqn (1)) as: $[(OAr)Sn(\mu\text{-}NMe_2)]_2$ where OAr = *o*MP (**1**), *o*PP (**2**), *o*BP (**3**), DMP (**4**), DIP (**5**), DBP (**6**) and for the homoleptic compounds (eqn (2)) as a mixture of polymers $[Sn(\mu\text{-}OAr)_2]_\infty$ [where OAr = *o*MP (**7**), *o*PP (**8**)], dinuclear $[(OAr)Sn(\mu\text{-}OAr)]_2$ (where OAr = *o*BP (**9**), DMP (**10**) or DIP/$HNMe_2$ (**11**)), and mononuclear $[Sn(DBP)_2]$ (**12**), species. Solution precipitation (SPPT) and electrospinning (ES) routes were undertaken using these novel compounds in an attempt to generate SnO_x nanowires. The various results of these studies will be presented.

$$[Sn(NMe_2)_2]_2 + 2\ H\text{-}OAr \longrightarrow [(OAr)Sn(\mu\text{-}NMe_2)]_2 + 2\ HNMe_2 \tag{1}$$

$$\boxed{\text{OAr} = o\text{MP (1), }o\text{PP (2), }o\text{BP (3), DMP (4), DIP (5), DBP (6)}}$$

$$[Sn(NMe_2)_2]_2 + 4\ H\text{-}OAr \longrightarrow [Sn(OAr)_2]_z + 4\ HNMe_2 \tag{2}$$

$$\boxed{\begin{array}{l} z = \infty:\ \text{OAr} = o\text{MP (7), }o\text{PP (8);} \\ z = 2:\ \text{OAr} = o\text{BP (9), DMP (10),} \\ \text{DIP/HNMe}_2\text{ (11);}\ \ z = 1:\ \text{OAr} = \text{DBP (12)} \end{array}}$$

Experimental section

All reactions were performed under a dry, inert atmosphere using standard Schlenk line and glovebox techniques. The following chemicals were used as received from Aldrich: $SnCl_2$, $LiNMe_2$, H-*o*MP, H-*o*PP, H-*o*BP, H-DMP, H-DIP, H-DBP. All anhydrous solvents were used as received (Aldrich) in Sure/Seal™ bottles. $[Sn(NMe_2)_2]_2$ was synthesized from the reaction of $SnCl_2$ and two equivalents of $LiNMe_2$ in THF at 0 °C.[27,28]

General instrumentation

FT-IR spectral data were obtained on a Nicolet 6700 FTIR spectrometer using KBr pellets pressed under an argon atmosphere and handled under an atmosphere of flowing nitrogen. Elemental analyses were performed on a Perkin-Elmer 2400 CHN-S/O elemental analyzer. All NMR samples were prepared using crystalline material handled under an argon atmosphere and then flame sealed under vacuum. Spectra were collected on a Bruker Avance 500 NMR spectrometer, using a 5 mm inverse probe, under standard experimental conditions: ^1H analysis was performed with a 4-second recycle delay at 16 scans; spectra were referenced to the toluene-d_8 peak at 2.09 ppm; ^{13}C spectra were obtained with a 10-second recycle delay and 4k scans and referenced to the methyl peak of the toluene-d_8 at 20.5 ppm; ^{119}Sn solution NMR analysis was performed with a 4–second recycle delay, and spectra were externally referenced to the secondary standard aqueous 1 M $SnMe_4$ at 0 ppm.

General synthesis

Due to the similarity of synthesis a general method is presented with particular details presented for each complex. To a stirring solution of $[Sn(NMe_2)_2]_2$ in toluene, the appropriate equivalent of the desired H-OAr was added, which immediately turned the reaction mixture to a dark yellow to orange color depending on the H-OAr used. The reaction mixtures were stirred for 12 h. For those reactions that formed a small precipitate, it was removed by centrifugation. The reaction or mother liquor was set aside open to the glovebox atmosphere to allow the volatile fraction to slowly evaporate until crystals formed. All analyses were performed on the crystalline material.

[(*o*MP)Sn(μ-NMe₂)]₂ (1). Used $[Sn(NMe_2)_2]_2$ (0.500 g, 1.21 mmol), H-*o*MP (0.261 g, 2.42 mmol), and ~10 mL toluene. Yield 68.9% (0.450 g). FTIR (KBr pellet, cm^{-1}) 2962(s), 2929(sh, s), 2895(sh, s), 2860(sh, s), 2729(w), 2703(w), 2589(w), 2364(w), 2340(w), 2254(w), 2118(w), 1884(w), 1649(m), 1597(m), 1466(s), 1382(s), 1357(s), 1234(s), 1190(s), 1046(s), 1023(s), 933(s), 859(w), 841(m), 792(m), 778(sh, m), 756(s), 728(w), 616(s), 569(s), 560(sh, s), 489(s), 472(sh, s), 455(sh, s), 413(sh, s). ^1H NMR (500.1 MHz, tol-d_8): δ 7.20

(1 H, d, $\mathrm{OC_6}H_4\mathrm{(CH_3)}$, $J_{\mathrm{H–H}}$ = 3.0 Hz), δ 7.08 (1 H, t, $\mathrm{OC_6}H_4\mathrm{(CH_3)}$, $J_{\mathrm{H–H}}$ = 5.6 Hz), δ 6.82 (1 H, t, $\mathrm{OC_6}H_4\mathrm{(CH_3)}$, $J_{\mathrm{H–H}}$ = 5.6 Hz), 6.71 (1 H, d, $\mathrm{OC_6}H_4\mathrm{(CH_3)}$, $J_{\mathrm{H–H}}$ = 3.2 Hz), 2.34 (3 H, s, $\mathrm{OC_6H_4(C}H_3\mathrm{))}$, 2.33 (6 H, s, $\mathrm{N(C}H_3\mathrm{)_2}$). ^{13}C NMR (100.1 MHz, tol-d$_8$): δ 161.2, 131.4, 127.1, 118.5, 117.1 ($\mathrm{O}C_6\mathrm{H_4(CH_3))}$), 40.9 ($\mathrm{N(}C\mathrm{H_3)_2}$), 18.4 ($\mathrm{OC_6H_4(}C\mathrm{H_3))}$). Anal. Calcd for $\mathrm{C_{18}H_{26}N_2O_2Sn_2}$ (M_{W} = 539.96): C, 40.04; H, 4.85; N, 5.21. Found: C, 40.53; H, 4.66; N, 4.23.

[(*o*PP)Sn(μ-NMe$_2$)]$_2$ (2). Used [Sn(NMe$_2$)$_2$]$_2$ (0.500 g, 1.21 mmol), H-*o*PP (0.329 g, 2.42 mmol), and ~10 mL toluene. Yield 72.1% (0.519 g). FTIR (KBr pellet, cm^{-1}) 3070(m), 3060(sh, m), 3044(sh, m), 2998(s), 2956(s), 2933(sh, s), 2935 (sh, s), 2913(sh, s), 2860(s), 2831(sh, s) 2782(s), 1590(s), 1572(s), 1480(s), 1458(s), 1441(sh, s), 1403(s), 1380(m), 1360 (m), 1340(s), 1285(s), 1271(s), 1258(s), 1242(sh, s), 1217(sh, s), 1188(s), 1155(m), 1153(m), 1123(s), 1079(s), 1036(s), 967(w), 927(m), 893(s), 874(sh, m), 845(sh, s), 838(sh, s), 758(s), 739(s), 722(s), 702(m), 602(s), 577(m), 570(sh, m), 562(sh, m), 530(m), 495(m), 460(s), 441(s), 408(s), 406(sh, s). ^{1}H NMR (500.1 MHz, tol-d$_8$): δ 7.29 (1 H, d, $\mathrm{OC_6}H_4\mathrm{(CH(CH_3)_2)}$, $J_{\mathrm{H–H}}$ = 2.8 Hz), 6.89 (1 H, t, $\mathrm{OC_6}H_4\mathrm{(CH(CH_3)_2)}$, $J_{\mathrm{H–H}}$ = 6.0 Hz), 6.71 (1 H, d, $\mathrm{OC_6}H_4\mathrm{(CH(CH_3)_2)}$, $J_{\mathrm{H–H}}$ = 3.0 Hz), 3.62 (1 H, sept, $\mathrm{OC_6H_4(C}H\mathrm{(CH_3)_2)}$, $J_{\mathrm{H–H}}$ = 5.6 Hz), 2.39 (6 H, s, $\mathrm{N(C}H_3\mathrm{)_2}$), 1.33 (6 H, d, $\mathrm{OC_6H_4(CH(C}H_3\mathrm{)_2)}$, $J_{\mathrm{H–H}}$ = 4.4 Hz). ^{13}C NMR (100.1 MHz, tol-d$_8$): δ 160.4, 126.7, 126.4, 118.9, 117.4 ($\mathrm{O}C_6\mathrm{H_4(CH(CH_3)_2)}$, 41.0 ($\mathrm{N(}C\mathrm{H_3)_2}$), 27.3 ($\mathrm{OC_6H_4(}C\mathrm{H(CH_3)_2)}$, 23.4 ($\mathrm{OC_6H_4(CH(}C\mathrm{H_3)_2)}$. Anal. Calcd for $\mathrm{C_{22}H_{34}N_2O_2Sn_2}$ (M_{W} = 595.94): C, 44.34; H, 5.75; N, 4.70. Found: C, 44.85; H, 5.65; N, 3.57.

[(*o*BP)Sn(μ-NMe$_2$)$_2$]$_2$ (3). Used [Sn(NMe$_2$)$_2$]$_2$ (0.500 g, 1.21 mmol), H-*o*BP (0.365 g, 2.42 mmol), and ~10 mL toluene. Yield 83.5% (0.629 g). FTIR (KBr pellet, cm^{-1}) 2959(s), 2921 (sh, s), 2888(sh, s), 2859(sh, s), 2721(sh, m), 1467(s), 1454(sh, s), 1385(s), 1362(s), 1231(s), 1187(s), 1102(w), 1050(w), 1023 (m), 955(s), 914(s), 900(s), 841(w), 804(w), 754(s), 684(w), 584(s), 559(sh, s), 463(s), 449(sh, m), 432(w). ^{1}H NMR (500.1 MHz, tol-d$_8$): δ 7.39 (1 H, d, $\mathrm{OC_6}H_4\mathrm{(C(CH_3)_3)}$, $J_{\mathrm{H–H}}$ = 3.0 Hz), 7.06 (1 H, t, $\mathrm{OC_6}H_4\mathrm{(C(CH_3)_3)}$, $J_{\mathrm{H–H}}$ = 6.0 Hz), 6.85 (1 H, t, $\mathrm{OC_6}H_4\mathrm{(C(CH_3)_3)}$, $J_{\mathrm{H–H}}$ = 6.0 Hz), 6.59 (1 H, d, $\mathrm{OC_6}H_4\mathrm{(C(CH_3)_3)}$, $J_{\mathrm{H–H}}$ = 3.0 Hz), 2.49 (3 H, s, $\mathrm{N(C}H_3\mathrm{)_2}$), 1.57 (9 H, s, $\mathrm{OC_6H_4(C(C}H_3\mathrm{)_3))}$. ^{13}C NMR (100.1 MHz, tol-d$_8$): δ 161.5, 139.1, 127.4, 127.1, 118.9, 118.7 ($\mathrm{O}C_6\mathrm{H_4(C(CH_3)_3))}$, 42.2 ($\mathrm{N(}C\mathrm{H_3)_2}$), 35.2 ($\mathrm{OC_6H_4(}C\mathrm{(CH_3)_3))}$, 30.2 ($\mathrm{OC_6H_4(C(}C\mathrm{H_3)_3))}$. Anal. Calcd for $\mathrm{C_{24}H_{38}N_2O_2Sn_2}$ (M_{W} = 624.00): C, 46.20; H, 6.14; N, 4.49. Found: C, 46.66; H, 6.28; N, 4.32.

[(DMP)Sn(μ-NMe$_2$)]$_2$ (4). Used [Sn(NMe$_2$)$_2$]$_2$ (0.500 g, 1.21 mmol), H-DMP (0.295 g, 2.42 mmol), and ~10 mL toluene. Yield 74.8% (0.513 g). FTIR (KBr pellet, cm^{-1}) 3062 (s), 3039(sh, s), 3009(s), 2958(s), 2941(sh, s), 2902(s), 2864(sh, s), 2788(s), 2772(m), 1589(s), 1464(s), 1419(s), 1372(m), 1290(m), 1262(s), 1219(s), 1200(sh, s), 1159(sh, m), 1124(m), 1094(s), 1037(s), 981(w), 951(sh, w), 913(w), 900(w), 843(s), 804(m), 763(s), 742(m), 684(m), 575(s), 563(s), 522(s), 507(sh, s), 464(s), 422(sh, m). ^{1}H NMR (500.1 MHz, tol-d$_8$): δ 7.07 (2 H, d, $\mathrm{OC_6}H_3\mathrm{((CH_3)_2)}$, $J_{\mathrm{H–H}}$ = 2.8 Hz), 6.76 (1 H, t, $\mathrm{OC_6}H_3\mathrm{((CH_3)_2)}$, $J_{\mathrm{H–H}}$ = 5.6 Hz), 2.40 (6 H, s, $\mathrm{N(C}H_3\mathrm{)_2}$), 2.29 (6 H, s, $\mathrm{OC_6}H_3\mathrm{((C}H_3\mathrm{)_2)}$. ^{13}C NMR (100.1 MHz, tol-d$_8$): δ 160.4, 126.2, 118.1 ($\mathrm{O}C_6\mathrm{H_3((CH_3)_2))}$, 40.7 ($\mathrm{N(}C\mathrm{H_3)_2}$), 20.9 ($\mathrm{OC_6H_3((}C\mathrm{H_3)_2))}$. Anal. Calcd for $\mathrm{C_{20}H_{30}N_2O_2Sn_2}$ (M_{W} = 567.89): C, 42.30; H, 5.32; N, 4.93. Found: C, 42.36; H, 5.26; N, 4.28.

[(DIP)Sn(μ-NMe$_2$)]$_2$ (5). Used [Sn(NMe$_2$)$_2$]$_2$ (0.500 g, 1.21 mmol), H-DIP (0.431 g, 2.42 mmol), and ~10 mL toluene. Yield 62.6% (0.514 g). FTIR (KBr pellet, cm^{-1}) 3055(s), 3031(m), 3019(sh, m), 2959(s), 2925(sh, s), 2865(s), 1596 (s), 1460(s), 1442(s), 1426(s), 1381(m), 135(m), 1322(m), 1256(s), 1205(s), 1196(sh, s), 1158(w), 1149(m), 1109(m), 1097(sh, m), 1069(m), 1045(w), 1034(m), 1003(m), 932(w), 883(m), 842(s), 796(w), 752(s), 702(s), 677(w), 620(m), 570(m), 541(s), 461(sh, m), 420(m). ^{1}H NMR (500.1 MHz, tol-d$_8$): δ 7.14 (2 H, d, $\mathrm{OC_6}H_3\mathrm{((CH(CH_3)_2)_2)}$, $J_{\mathrm{H–H}}$ = 3.0 Hz), 6.92 (1 H, t, $\mathrm{OC_6}H_3\mathrm{((CH(CH_3)_2)_2)}$, $J_{\mathrm{H–H}}$ = 6.0 Hz), 3.52 (1 H, m, $\mathrm{OC_6H_3((C}H\mathrm{(CH_3)_2)_2)}$, $J_{\mathrm{H–H}}$ = 5.6 Hz), 2.56 (6 H, s, $\mathrm{N(C}H_3\mathrm{)_2}$), 1.27 (12 H, d, $\mathrm{OC_6H_3((CH(C}H_3\mathrm{)_2)_2)}$, $J_{\mathrm{H–H}}$ = 5.6 Hz). ^{13}C NMR (100.1 MHz, tol-d$_8$): δ 156.5, 123.7, 119.1 ($\mathrm{O}C_6\mathrm{H_3((CH(CH_3)_2)_2))}$, 40.9($\mathrm{N(}C\mathrm{H_3)_2}$), 27.9 ($\mathrm{OC_6H_3((}C\mathrm{H(CH_3)_2)_2))}$, 24.3 ($\mathrm{OC_6H_3((CH(}C\mathrm{H_3)_2)_2))}$. Anal. Calcd for $\mathrm{C_{28}H_{46}N_2O_2Sn_2}$ (M_{W} = 672.00): C, 50.05; H, 5.70; N, 4.17. Found: C, 48.29; H, 6.64; N, 3.99.

[(DBP)Sn(μ-NMe$_2$)]$_2$ (6). Used [Sn(NMe$_2$)$_2$]$_2$ (0.500 g, 1.21 mmol), H-DBP (0.499 g, 2.42 mmol), and ~10 mL toluene. Yield 78.5% (0.698 g). FTIR (KBr pellet, cm^{-1}) 3056(m), 3054(sh, m), 3071(m), 3019(m), 2954(s), 2900(sh, s), 2870(sh, s), 2799(sh, m), 1580(m), 1475(m), 1468(sh, m), 1444(m), 1425(m), 1399(s), 1383(s), 1359(m), 1351(m), 1319(sh, w), 1258(s), 1219(s), 1190(s), 1151(m), 1119(s), 1104(s), 1067(sh, w), 1036(m), 1009(sh, w), 947(w), 919(w), 886(s), 847(s), 809(s), 797(sh, m), 755(s), 701(w), 634(m), 601(w), 577(w), 533(m), 459(m), 437(s), 426(sh, s), 403(s). Anal. Calcd for $\mathrm{C_{32}H_{54}N_2O_2Sn_2}$ (M_{W} = 736.45): C, 52.49; H, 7.39; N, 3.80. Found: C, 52.60; H, 7.41; N, 3.45.

[Sn(μ-oMP)$_2$]$_\infty$ (7). Used [Sn(NMe$_2$)$_2$]$_2$ (0.500 g, 1.21 mmol), H-*o*MP (0.522 g, 4.83 mmol), and ~10 mL toluene. Yield 19.2% (0.154 g). FTIR (KBr pellet, cm^{-1}) 2953(s), 2922(sh, s), 2895(sh, s), 2860(sh, s), 2703(w), 2367(w), 1888(w), 1653(m), 1592(m), 1466(s), 1382(s), 1357(s), 1233(s), 1188(s), 1092(s), 1046(m), 1023(m), 944(s), 843(m), 757(s), 729(w), 613(sh, s), 565(s), 473(s), 418(sh, m). ^{1}H NMR (500.1 MHz, tol-d$_8$): δ 7.02 (1 H, d, $\mathrm{OC_6}H_4\mathrm{(CH_3)}$, $J_{\mathrm{H–H}}$ = 3.0 Hz), 6.95 (1 H, t, $\mathrm{OC_6}H_4\mathrm{(CH_3)}$, $J_{\mathrm{H–H}}$ = 6.0 Hz), 6.77 (2H, m, $\mathrm{OC_6}H_4\mathrm{(CH_3))}$, 2.16 (3H, s, $\mathrm{OC_6}H_4\mathrm{(CH_3))}$. ^{13}C NMR (100.1 MHz, tol-d$_8$): δ 156.9, 131.5, 127.3, 120.9, 120.4 ($\mathrm{O}C_6\mathrm{H_4(CH_3))}$, 18.1 ($\mathrm{OC_6H_4(}C\mathrm{H_3))}$. Anal. Calcd for $\mathrm{C_{14}H_{14}O_2Sn}$ (M_{W} = 332.97): C, 50.50; H, 4.24; N, 0.00. Found: C, 51.06; H, 4.29; N, 1.07.

[Sn (μ-oPP)$_2$]$_\infty$ (8). Used [Sn(NMe$_2$)$_2$]$_2$ (0.500 g, 1.21 mmol), H-*o*PP (0.658 g, 4.83 mmol), and ~10 mL toluene. Yield 55.1% (0.518 g). FTIR (KBr pellet, cm^{-1}) 3064(m), 3029(m), 2961(s), 2868(sh, m), 1591(m), 1488(s), 1444(s), 1382(m), 1361(m), 1344(m), 1285(sh, s), 1252(s), 1191(m), 1149(s), 1111(w), 1085(m), 1035(m), 1008(sh, w), 925(s), 888(m), 838(s), 814(sh, s), 775(sh, s), 758(s), 689(sh, w), 637(w), 592(m), 578(m), 539(w), 488(w), 447(w). ^{1}H NMR

(500.1 MHz, tol-d$_8$): δ 7.15 (1 H, d, $OC_6\mathit{H}_3((CH(CH_3)_2)_2)$, J_{H-H} = 3.2 Hz), 6.95 (1 H, t, $OC_6\mathit{H}_3((CH(CH_3)_2)_2)$, J_{H-H} = 6.0 Hz), 6.83 (1 H, t, $OC_6\mathit{H}_3((CH(CH_3)_2)_2)$, J_{H-H} = 6.0), 6.53 (1 H, mult, $OC_6\mathit{H}_3((CH(CH_3)_2)_2)$), 3.66 (1 H, sept, $OC_6H_3((C\mathit{H}(CH_3)_2)_2)$, J_{H-H} = 5.4 Hz), 1.20 (6 H, d, $OC_6H_3((CH(C\mathit{H}_3)_2)_2)$, J_{H-H} = 5.6 Hz). ^{13}C NMR (100.1 MHz, tol-d$_8$): δ 148.9, 139.3, 136.4, 126.7, 126.5, 129.9 ($O\mathit{C}_6H_3((CH(CH_3)_2)_2)$, 26.94 ($OC_6H_3((\mathit{C}H(CH_3)_2)_2)$, 24.10 ($OC_6H_3((CH(\mathit{C}H_3)_2)_2)$. Anal. Calcd for $C_{18}H_{22}O_2Sn$ (M_W = 389.08): C, 55.57, H, 5.70. Found: C, 55.81; H, 6.03.

[(*o*BP)Sn(μ-*o*BP)]$_2$ (9). Used $[Sn(NMe_2)_2]_2$ (0.500 g, 1.21 mmol), H-*o*BP (0.730 g, 4.83 mmol), and ~10 mL toluene. Yield 60.8% (0.613 g). FTIR (KBr pellet, cm^{-1}) 3055(m), 3008 (s), 2966(s), 2904(s), 2868(s), 2825(sh, m), 2783(m), 1907(w), 1871(w), 1592(s), 1572(sh, m), 1482(s), 1451(s), 1430(s), 1406(m), 1372(w), 1281(sh, s), 1272(sh, s), 1256(s), 1184(s), 1152(m), 1125(m), 1111(s), 1045(s), 1037(s), 981(m), 901(m), 856(s), 754(s), 713(s), 597(s), 566(s), 536(s), 472(s). ^{1}H NMR (500.1 MHz, tol-d$_8$): δ 7.36 (1 H, d, $OC_6\mathit{H}_4(C(CH_3)_3)$, J_{H-H} = 3.2 Hz), 7.01 (1 H, t, $OC_6\mathit{H}_4(C(CH_3)_3)$, J_{H-H} = 6.0 Hz), 6.88 (1 H, d, $OC_6\mathit{H}_4(C(CH_3)_3)$, J_{H-H} = 2.8 Hz), 6.82 (1 H, t, $OC_6\mathit{H}_4(C(CH_3)_3)$, J_{H-H} = 6.0 Hz), 1.77 (2 H, s, $HNMe_2$), 1.57 (9 H, s, $OC_6H_4(C(C\mathit{H}_3)_3)$). ^{13}C NMR (100.1 MHz, tol-d$_8$): δ 160.0, 139.5, 127.5, 127.2, 119.9, 119.1 ($O\mathit{C}_6H_4(C(CH_3)_3)$), 36.1, 35.2 ($OC_6H_4(\mathit{C}(CH_3)_3)$), 30.4 ($OC_6H_4(C(\mathit{C}H_3)_3)$). Anal. Calcd for $C_{20}H_{26}O_2Sn$ (M_W = 417.13): C, 57.59, H, 6.28. Found: C, 61.09; H, 7.50; N, 1.63.

[(DMP)Sn(μ-DMP)]$_2$·tol (10). Used $[Sn(NMe_2)_2]_2$ (0.500 g, 1.21 mmol), H-DMP (0.590 g, 4.83 mmol), and ~10 mL toluene. Yield 78.6% (0.685 g). FTIR (KBr pellet, cm^{-1}) 3062(m), 3011(m), 2957(s), 2903(s), 2853(m), 2727(m), 2027(w), 1921(w), 1852(w), 1785(w), 1660(w), 1588(s), 1494(s), 1465(s), 1418(s), 1378(m), 1322(w), 1299(m), 1262(s), 1233(sh, m), 1218(s), 1182(s), 1092(s), 1029(m), 981(w), 914(w), 861(sh, m), 835(s), 781(sh, m), 769(s), 760(s), 742(m), 731(m), 698(w), 692(s), 680(s), 575(s), 556(m), 522(s), 507(s), 463(w), 430(m), 412(m). ^{1}H NMR (500.1 MHz, tol-d$_8$): δ 6.95 (2 H, d, $OC_6\mathit{H}_3((CH_3)_2)$, J_{H-H} = 3.0 Hz), 6.74 (1 H, t, $OC_6\mathit{H}_3((CH_3)_2)$, J_{H-H} = 6.0 Hz), and 2.28 (6 H, s, $OC_6H_3((C\mathit{H}_3)_2)$). ^{13}C NMR (100.1 MHz, tol-d$_8$): δ 135.4, 129.1, 120.4 ($O\mathit{C}_6H_3((CH_3)_2)$), 19.2 ($OC_6H_3((\mathit{C}H_3)_2)$). Anal. Calcd for $C_{32}H_{36}O_4Sn$ (M_W = 361.02): C, 53.23, H, 5.03. Found: C, 52.92; H, 5.09.

[(DIP)Sn(μ-DIP)$_2$Sn(DIP)(HNMe$_2$)] (11). Used $[Sn(NMe_2)_2]_2$ (0.500 g, 1.21 mmol), H-DIP (0.862 g, 4.83 mmol), and ~10 mL toluene. Yield 50.8% (0.580 g). FTIR (KBr pellet, cm^{-1}) 3055(s), 3020(m), 2960(s), 2865(s), 2008(w), 1988(w), 1923(w), 1890(w), 1864(w), 1839(w), 1788(w), 1696(w), 1648(w), 1628(w), 1596(s), 1460(s), 1443(sh, s), 1423(s), 1381(s), 1354(s), 1323(s), 1256(s), 1206(s), 1119(s), 1158(s), 1149(m), 1096(sh, m), 1069(m), 1045(sh, m), 1033(s), 1003(s), 932(m), 883(s), 842(s), 796(m), 752(s), 701(s), 677(m), 620(m), 583(sh, w), 571(m), 541(s), 460(w), 421(w). ^{1}H NMR (500.1 MHz, tol-d$_8$): δ 7.07 (2 H, d, $OC_6\mathit{H}_3((CH(CH_3)_2)_2)$, J_{H-H} = 3.2 Hz), 6.88 (1 H, t, $OC_6\mathit{H}_3((CH(CH_3)_2)_2)$, J_{H-H} = 3.2 Hz), 3.53 (2 H, s(br), $OC_6H_3((C\mathit{H}(CH_3)_2)_2)$), 1.90 (2 H, s, $H(N(C\mathit{H}_3)_2)]_2$), 1.18 (12 H, d, $OC_6H_3((CH(C\mathit{H}_3)_2)_2)$, J_{H-H} = 5.2 Hz). ^{13}C NMR (100.1 MHz, tol-d$_8$): δ 137.4, 129.3, 128.6, 137.7 ($O\mathit{C}_6H_3((CH(CH_3)_2)_2)$), 36.1 ($N(\mathit{C}H_3)_2$), 27.6 ($OC_6H_3((\mathit{C}H(CH_3)_2)_2)$), 24.5 ($OC_6H_3((CH(\mathit{C}H_3)_2)_2)$). Anal. Calcd for $C_{50}H_{75}NO_4Sn_2$ (M_W = 991.49): C, 60.57, H, 7.62, N, 1.41. Found: C, 61.06; H, 7.59; N, 1.15.

[(DBP)$_2$Sn] (12). Used $[Sn(NMe_2)_2]_2$ (0.500 g, 1.21 mmol), H-DBP (0.998 g, 4.83 mmol), and ~10 mL toluene. Yield 85.3% (1.09 g). FTIR (KBr pellet, cm^{-1}) 3642(s), 3061(s), 2956(s), 2908(sh, s), 2041(w), 1910(w), 1851(w), 1795(w), 1695(w), 1651(w), 1579(m), 1480(s), 1462(s), 1425(sh, s), 1403(s), 1362(w), 1315(w), 1259(m), 1213(s), 1144(w), 1115(m), 1100(m), 1040(w), 1024(w), 923(w), 882(m), 846(s), 811(s), 798(sh, m), 762(s), 752(s), 647(m), 638(m), 576(m), 536(m), 474(sh, w), 450(s), 421(m), 408(m). ^{1}H NMR (500.1 MHz, tol-d$_8$): δ 7.32 (2H d, $OC_6\mathit{H}_3((C(CH_3)_3)_2)$, J_{H-H} = 3.2 Hz), 6.85 (1 H, t, $OC_6\mathit{H}_3((C(CH_3)_3)_2)$, J_{H-H} = 6.0 Hz), 1.57 (18 H, s, $OC_6H_3((C(C\mathit{H}_3)_3)_2)$. ^{13}C NMR (100.1 MHz, tol-d$_8$): δ 139.8, 119.4 ($O\mathit{C}_6H_3((C(CH_3)_3)_2)$), 35.3 ($OC_6H_3((\mathit{C}(CH_3)_3)_2)$), 33.1 ($OC_6H_3((C(\mathit{C}H_3)_3)_2)$). Anal. Calcd for $C_{28}H_{42}O_2Sn$ (MW = 529.34): C, 63.53, H, 8.00, N, 0.00. Found: C, 63.52; H, 8.05; N, 0.82.

General X-ray crystal structure information[29]

Crystals were mounted from a pool of Fluorolube™ and immediately placed in a cold N_2 vapor stream, on a Bruker AXS diffractometer equipped with a SMART 1000 CCD detector using graphite monochromatized MoKα radiation (λ = 0.7107 Å) or a Bruker AXS diffractometer equipped with a APEX II detector. Lattice determination and data collection As well as data reduction and corrected for absorption was performed using the appropriate software suite, either SMART or APEX II.

Structures were solved by direct methods that yielded the heavy atoms, along with a number of the lighter atoms or by using the PATTERSON method, which yielded the heavy atoms. Subsequent Fourier syntheses yielded the remaining light-atom positions. The hydrogen atoms were fixed in positions of ideal geometry and refined using Shelxl-97 software. The final refinement of each compound included anisotropic thermal parameters for all non-hydrogen atoms. All final CIF files were checked at http://www.iucr.org/. Additional information concerning the data collection and final structural solutions can be found in the ESI† or by accessing CIF files through the Cambridge Crystallographic Data Base. Data collection parameters for **1–12** are given in Table 1. For **7**, one disordered toluene was removed using SQUEEZE in the PLATON software suite. Structure plots for each of the compounds discussed in this report (hetero-, homoleptic, and oxide compounds) are shown in the ESI† (Fig. S1–S15†). Plots of representative structure types are shown in Fig. 1–5.

Solution precipitation (SPPT) route

A SPPT route was used to generate all nanomaterials using crystalline materials. The desired precursor (1 mmol) dissolved in oleylamine (~2 mL) was added to a heated, stirring solution of octadecene (~10 mL) in a glass, three-neck, round bottom flask. After heating at reflux for 45 min, the reaction was allowed to cool to room temperature and the resulting powder was isolated by centrifugation. The grey precipitate was then washed three

Table 1 Data collection parameters for **1–12** and oxide materials (**S1–S3**)

Compound	**1**	**2**	**3**	**4**
Chemical formula	$C_{18}H_{26}N_2O_2Sn_2$	$C_{16}H_{22}N_2OSn$	$C_{24}H_{38}N_2O_2Sn_2$	$C_{20}H_{30}N_2O_2$ Sn_2
Formula weight	539.79	377.05	623.94	567.84
Temp (K)	173(2)	173(2)	173(2)	173(2)
Space group	Monoclinic, $C2/c$	Triclinic, $P\bar{1}$	Triclinic, $P\bar{1}$	Monoclinic, $P2(1)/n$
a (Å)	26.984(3)	8.1411(12)	8.2967(7)	12.3543(19)
b (Å)	7.4491(7)	9.4382(14)	11.3895(9)	14.471(2)
c (Å)	21.522(2)	11.1451(17)	21.6629(18)	13.135(2)
α (°)		85.095(2)	89.6130(10)	
β (°)	106.458(2)	82.534(2)	80.5720(10)	104.226(3)
γ (°)		88.505(2)	79.6220(10)	
V (Å^3)	4148.9(7)	845.9(2)	1985.8(3)	2276.2(6)
Z	8	2	3	4
D_{calcd} (Mg m^{-3})	1.729	1.480	1.565	1.657
μ (Mo, Kα) (mm^{-1})	2.419	1.508	1.907	2.209
(R_{int})	0.035	0.011	0.027	0.047
$R_1{}^a$ (%) (all data)	3.32 (4.00)	1.96 (2.01)	3.39 (4.49)	4.06 (5.37)
w$R_2{}^b$ (%) (all data)	6.89 (7.16)	4.91 (4.93)	7.00 (7.45)	9.08 (9.67)

Compound	**5**	**6**	**7**	**8**
Chemical formula	$C_{28}H_{46}N_2O_2$ Sn_2	$C_{32}H_{54}N_2O_2Sn_2$	$C_{70}H_{70}O_{10}Sn_5$	$C_{72}H_{88}O_8Sn_4$
Formula weight	680.05	736.15	1664.71	1556.18
Temp (K)	173(2)	203(2)	188(2)	173(2)
Space group	Monoclinic, $P2(1)/c$	Monoclinic, $P2(1)/c$	Triclinic, $P\bar{1}$	Triclinic, $P\bar{1}$
a (Å)	9.9563(8)	15.0543(15)	11.166(2)	12.2459(8)
b (Å)	20.5582(17)	12.3130(12)	12.382(2)	12.5489(8)
c (Å)	15.2269(13)	18.4523(18)	26.605(5)	13.8878(9)
α (°)			99.731(2)	101.888(1)
β (°)	101.518(1)	100.9500(1)	92.217(2)	111.323(1)
γ (°)			111.074(2)	110.848(1)
V (Å^3)	3053.9(4)	3358.1(6)	3363 (11)	1713.48(19)
Z	4	4	2	1
D_{calcd} (Mg m^{-3})	1.479	1.456	1.644	1.507
μ (Mo, Kα) (mm^{-1})	1.660	1.516	1.887	1.492
R_{int}	0.021	0.019	0.018	0.017
$R_1{}^a$ (%) (all data)	2.06 (2.53)	2.11 (2.38)	3.48 (4.16)	2.59(3.01)
w$R_2{}^b$ (%) (all data)	4.87 (5.14)	5.37 (5.55)	8.39 (8.74)	6.49 (6.74)

Compound	**9**	**10**	**11**	**12**
Chemical formula	$C_{40}H_{52}O_4Sn_2$	$C_{39}H_{44}O_4Sn_2$	$C_{50}H_{75}NO_4Sn_2$	$C_{28}H_{42}O_2Sn$
Formula weight	834.20	814.12	991.49	529.31
Temp (K)	173(2)	203(2)	296(2)	203(2)
Space group	Triclinic, $P\bar{1}$	Monoclinic, $P2(1)/c$	Monoclinic, $P2(1)/c$	Monoclinic, $P2(1)/n$
a (Å)	8.36(4)	14.8587(11)	19.628(3)	13.856(5)
b (Å)	11.187(5)	10.8624(8)	13.8183(19)	13.874(5)
c (Å)	12.069(6)	22.554 (16)	19.431(3)	13.921(5)
α (°)	63.389(4)			
β (°)	71.234(5)	95.394(1)	111.156(6)	94.788(5)
γ (°)	84.577(5)			
V (Å^3)	953.9(8)	3624.1(5)	4915.1(13)	2666.8(15)
Z	1	4	4	4
D_{calcd} (Mg m^{-3})	1.452	1.492	1.340	1.318
μ (Mo, Kα) (mm^{-1})	1.346	1.416	1.057	0.978
R_{int}	0.016	0.025	0.063	0.020
$R_1{}^a$ (%) (all data)	1.97 (2.10)	2.97 (3.65)	3.60 (7.12)	2.30 (2.45)
w$R_2{}^b$ (%) (all data)	4.72 (4.80)	7.38(7.76)	7.39 (9.31)	6.02 (6.12)

Compound	**S1**	**S2**	**S3**
Chemical formula	$C_{46}H_{54}N_2O_8Sn_6$	$C_{45}H_{56}O_9Sn_6$	$C_{39}H_{60}O_7Sn_4$
Formula weight	1475.05	1453.04	1115.63
Temp (K)	173(2)	188(2)	173(2)
Space group	Monoclinic, $C2/c$	Triclinic, $P\bar{1}$	Orthorhombic, $Pbca$
a (Å)	15.9836(18)	12.3902(17)	22.7442(13)
b (Å)	19.1076(18)	13.1348(18)	16.4148(9)
c (Å)	15.9975(17)	16.511(2)	23.7362(13)
α (°)		88.778(2)	
β (°)	93.263(2)	72.1440(10)	

Table 1 *(Contd.)*

Compound	S1	S2	S3
γ (°)		75.5470(10)	
V (Å^3)	4877.8(9)	2472.2(6)	8861.7(9)
Z	4	2	8
D_{calcd} (Mg m^{-3})	2.0009	1.952	1.672
µ (Mo, Kα) (mm^{-1})	3.077	3.034	2.271
R_{int}	0.028	0.033	0.046
$R_1{}^a$ (%) (all data)	2.32 (2.87)	3.95 (5.48)	3.01 (4.13)
w$R_2{}^b$ (%) (all data)	9.11 (11.32)	10.30 (12.42)	9.38 (10.74)

[a] $R_1 = \Sigma \,||F_o| - |F_c||/\Sigma|F_o| \times 100$. [b] $wR_2 = [\Sigma w(F_o{}^2 - F_c{}^2)^2/\Sigma(w|F_o|^2)^2]^{1/2} \times 100$.

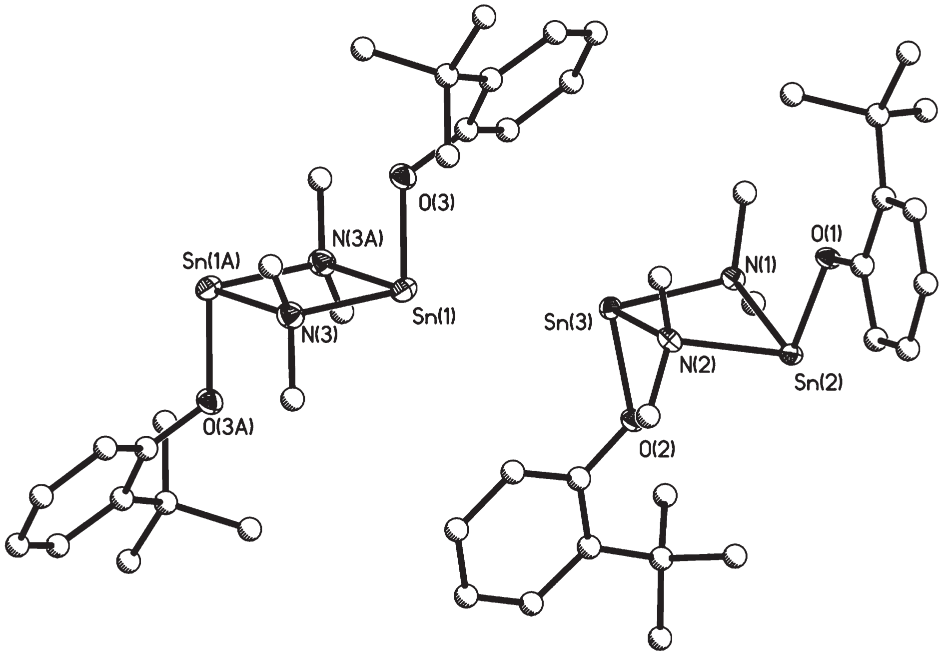

Fig. 1 Structure plot of **3**. Thermal ellipsoids of heavy atoms drawn at the 30% level with carbon atoms drawn as ball and stick for clarity. The two molecules located in the unit cell are shown.

times with chloroform and the resulting grey powder was allowed to dry at room temperature.

Transmission electron microscopy (TEM)

An aliquot of the nanopowder dispersed in chloroform was placed directly onto a holey carbon type-A, 200 mesh, copper TEM grid that was purchased from Ted Pella, Inc. The aliquot was then allowed to dry. The resultant particles were studied using a Philips CM 30 TEM operating at 300 kV accelerating voltage and equipped with a Thermo Noran System Six Energy Dispersive X-ray (EDX) System operating at 300 kV accelerating voltage.

Powder X-ray diffraction (PXRD)

Powder X-ray diffraction (XRD) was performed by a PANalytical X'Pert Pro XRD in the 2θ range of 10–100° at a scan rate of 0.15° s^{-1} on nanomaterials using a zero background holder. Representative patterns and calculated percentages are shown in the ESI† (Fig. S16–S19†).

Electrospinning (ES) synthesis

The appropriate precursor was dissolved in THF to generate a 0.66 M solution. This stock solution was transferred to a 3 mL syringe, fitted with an 18-gauge stainless steel needle (inner diameter of 0.965 mm). The syringe was fixed horizontally on a syringe pump (Model: MD-1000, Bioanalytical Systems Inc.). An electrode connected to a high voltage power supply (Model: DEL HVPS INST 230 30 KV, Spellman High Voltage Electronics Corporation) was attached to the tip of the metallic needle. A grounded stationary square collector (size 10 cm × 10 cm) consisting of a piece of graphene or cardboard square covered by a piece of clean aluminum foil was mounted 25 cm above the tip of the needle and used for the fiber collection.

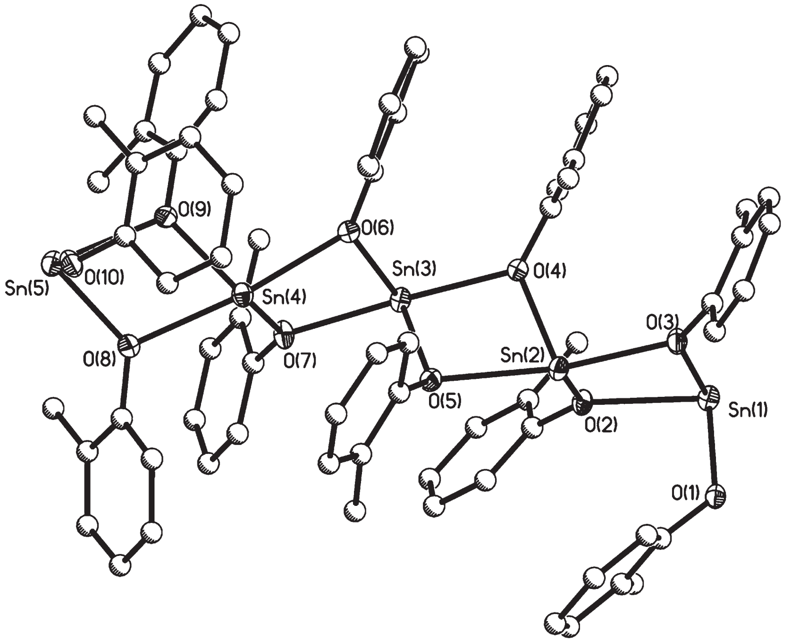

Fig. 2 Structure plot of growth moiety for polymeric **7**. Thermal ellipsoids of heavy atoms drawn at the 30% level with carbon atoms drawn as ball and stick for clarity.

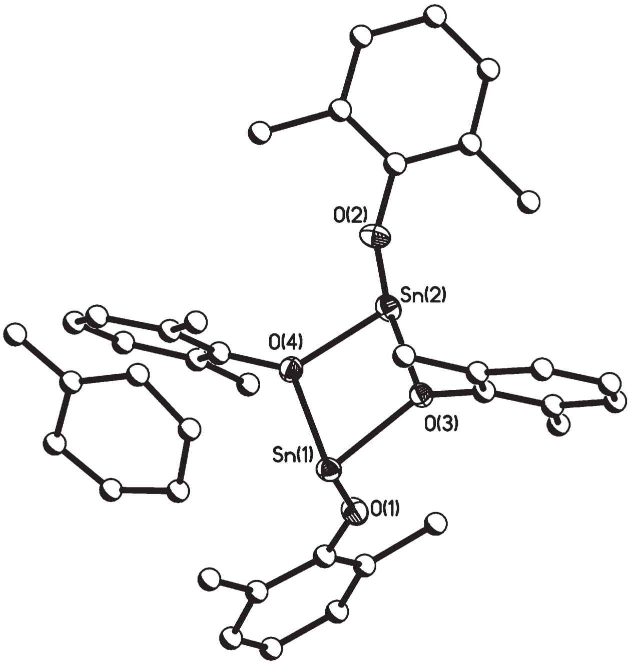

Fig. 3 Structure plot of **10**. Thermal ellipsoids of heavy atoms drawn at the 30% level with carbon atoms drawn as ball and stick for clarity.

Electrospinning to produce the Sn-bearing nanowires was carried out using the stock solution under the following conditions: flow rate (FR) was 0.9 mL h^{-1}; 15 kV, electric field (EF) was 0.6 kV cm^{-1}. The charge was applied and electrospinning was performed for ~60 min. An experimental setup can be found in the ESI (Fig. S20†).

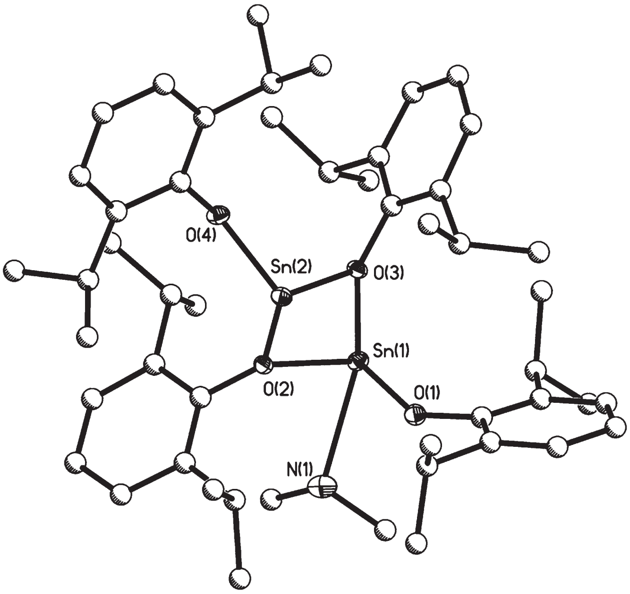

Fig. 4 Structure plot of **11**. Thermal ellipsoids of heavy atoms drawn at the 30% level with carbon atoms drawn as ball and stick for clarity.

Scanning electron microscopy (SEM)

A portion of electrospun material was cut from the Al foil or graphene substrate and fixed onto a SEM stub using double-sided carbon tape. The samples were then analyzed without further processing. Samples were imaged using a Hitachi S-5200 Nano SEM field emitter gun scanning electron microscope (FEGSEM). A PGT EDS detector and Spirit software was used for the acquisition of EDS spectra.

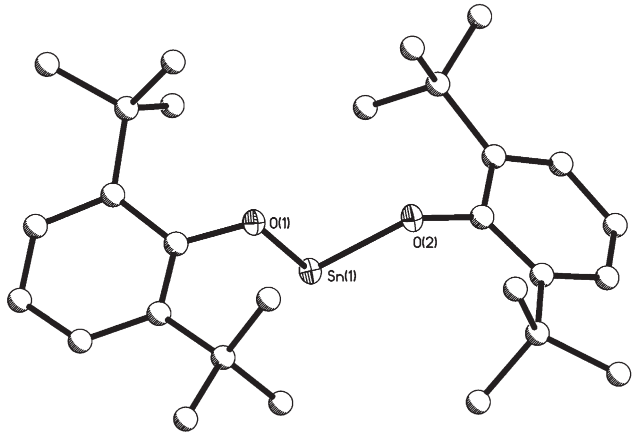

Fig. 5 Structure plot of **12**. Thermal ellipsoids of heavy atoms drawn at the 30% level with carbon atoms drawn as ball and stick for clarity.

Electrochemical analysis

Electrochemical studies on electrosprayed material were prepared by changing the working distance between the spray tip and the substrate to localize all the deposited material. Deposits were made on graphite paper (Grafoil™). All testing was conducted under an Ar atmosphere in 1 M TBAP in acetonitrile against a Ag/Ag^+ reference with Pt counter electrode. Cyclic voltammetry was performed at 25 mV s^{-1} at room temperature starting at 0.1 V *vs.* Ag/Ag+ (just above the Sn^0 to Sn^{2+} potential) and sweeping cathodically to look for SnO reduction to Sn^0 in the first sweep. Electrospun (ES) samples were punched with a 1 cm diameter punch to have a defined area of electrode for each measurement.

Results and discussion

The development of a series of Sn(II) compounds was necessary prior to investigating their utility for the production of SnO_x nanowires. Inert atmosphere methodologies were investigate to minimize water exposure thereby avoiding oxo intermediate formation throughout.[26,27] The synthesis and characterization of the various hetero- and homoleptic species isolated in this study are discussed below. This is followed by a discussion of the results for the SPPT and ES processing routes employing these compounds.

Heteroleptic

The initial precursors of interest were the ‘$Sn(OAr)(NMe_2)$’ compounds, since it was assumed the heteroleptic compounds would demonstrate an asymmetric decomposition upon thermal treatment which could lead to wire-like growth. The synthesis of these compounds was undertaken under an atmosphere of argon, through the addition of one equivalent of the desired H-OAr to a clear pale yellow solution of $[Sn(NMe_2)_2]_2$ dissolved in toluene (eqn (1)). Dependent on the HOAr employed, the reaction mixture changed to a dark yellow to orange color. Each reaction was stirred for 12 h and any precipitates formed were removed by centrifugation. The remaining soluble fraction was then set aside to slowly evaporate until crystals grew.

FTIR spectroscopic data of the products from these reactions indicated that a mixture of amide and alkoxide ligands were present with a loss of the 3000 cm^{-1} OH stretch. Two stretching modes for the ν(Sn–O) 476–466 cm^{-1} and ν(C–O)Sn in the range of 1030–1070 cm^{-1} should be observed for $Sn(OR)_x$ compounds;[30] however, due to the out-of-plane bends of the aryloxide ligands,[31–33] these stretches could not be unequivocally identified. The limited structural identification that could be discerned from the FTIR data led us to undertake single crystal X-ray experiments.

Table 1 shows the structural data parameters for **1–6**. Each of these compounds was found to adopt a dinuclear arrangement with a bridging NMe_2 and a terminal OAr ligand. The three coordinated Sn(II) metal centers have (N–μ)–Sn–(μ–N) angles of av 79.0° and O–Sn–(μ–N) av 90.85°. Fig. 1 shows compound **3** (two molecules located in the unit cell) as the representative member of the heteroleptic family isolated (see ESI† for all structures and packing diagrams). Prior to the isolation of **1–6**, the only OAr/amide complex reported was Sn(IV) species $(DBP\text{-}Me)_2Sn(NMe_2)_2$ (Sn-O distance av 1.98 Å, Sn–N distance av. 1.99 Å).[34] Other alkoxide amides include: $[((Me_3Si)_2N)Sn(\mu\text{-}OBu^t)]_2$[35] and $[((Me_3Si)_2N)Sn(\mu\text{-}OCH_2CH_2N(Me_2)^c)]_2$,[36] $[(OR^N)Sn(\mu\text{-}NMe_2)]_2$ where OR^N = 2-(((2,6-diisopropylphenyl)-imino)methyl-4,6-diiodophenolato).[37] The metrical data for **1–6** (see Table 2) are consistent with each other and the appropriate literature compounds.[34–37]

Purity of the bulk powders of the heteroleptic compounds was further investigated using elemental analysis. As is often noted for these types of compounds, obtaining useful elemental analyses is difficult due to the high volatility of the compounds, incomplete or premature decomposition of the precursor, or inclusion of solvents. Therefore, while the elemental analyses are within acceptable range for C and H, the percent of N for each sample was on the low end of the expected range. The one exception is compound **5** where significant more N was recorded than would be expected for the crystal structure; however, the C and H were considered low. Further, the values of the N percentage were extremely varied from sample to sample. This behavior implies a complex decomposition process is occurring for **5** which limits the utility of the data. Overall, the elemental analyses of **1–6** variability was attributed to the high volatility of the NMe_2 ligand, which makes determining purity difficult.

Therefore, further investigations were undertaken using ^1H, ^{13}C, and ^{119}Sn NMR experiments. The resonances of the ^1H spectra for **1–6** in tol-d_8 were found to be consistent with the respective OAr and the NMe_2 ligands in a 1 : 1 ratio and the ^{13}C NMR spectrum also confirmed the presence of only one set of OAr and NMe_2 ligands; however, a number of the OAr aryl peaks for these compounds were obscured by the tol-d_8 peaks. In an effort to elucidate the powder's solution behavior and purity, ^{119}Sn NMR [^{119}Sn 8.58% natural abundance, I = 1/2 and ^{117}Sn, 7.61% natural abundance, I = 1/2) spectra were collected and are tabulated in Table 3. Only one ^{119}Sn resonance was observed for **1–5**, ranging from −39 to −52 ppm. Compound **6** had too low a solubility to allow for meaningful analysis. A correlation between the chemical shift and the coordination number of the Sn has been previously proffered,[38] with

Table 2 Metrical data summary for **1–12**[a]

Compound	**1**	**2**	**3**	**4**	**5**	**6**
Distances (Å)						
Sn···Sn	3.30	3.46	3.35	3.33	3.31	3.41
Sn–(μ–N)	2.23	2.27	2.24	2.23	2.23	2.27
Sn–O	2.07	2.0719(14)	2.053(3)	2.05	2.06	2.09
Angle (°)						
Sn–μ–N–Sn	95.51	99.43(6)	96.99(12)	96.7	95.8	97.7
(N–μ)–Sn–(μ–N)	79.13	80.57(7)	79.50	78.5	79.7	76.6
O–Sn–(μ–N)	87.39	88.45	92.13	90.1	89.0	98.0
Compound	**7**	**8**	**9**	**10**	**11**	**12**
Distances (Å)						
Sn···Sn	3.65	3.57	3.53	3.52	3.57	—
Sn–μ–O	2.25	2.14	2.1695(16)	2.18	2.27	—
Sn–O	—	—	2.0624(17)	2.05	2.04	2.02
Angle (°)						
O–Sn–O	—	—	—	—	—	89.01(7)
(O–μ)–Sn–(O)	—	—	89.6	88.6	91.7	—
(μ–O)–Sn–(μ–O)	96.5	92.7	75.0	71.3	70.8	—
Sn–(μ–O)–Sn	110.1	107.4	105.01(7)	107.7	107.3	—
N–Sn–O	—	—	—	—	77.6(2)	—

[a] All values are averaged except when error bars are presented; — not present

Table 3 ^{119}Sn NMR data for **1–12**[a]

Compound	δ ^{119}Sn (tol-d_8)	Compound	δ ^{119}Sn (tol-d_8)
1	−42.426	**7**	−412.1
2	−43.249	**8**	−429.2 (75%), −490.3 (25%)
3	−39.349	**9**	−315.7 (3%) −323.0(97%) −329.1 (100% @50°C)
4	−44.772	**10**	−293.5
5	−52.598	**11**	−121.6 (9%) −340.5 (91%)
6	—	**12**	−219.0

[a] — insoluble.

3-coordinated Sn(II) alkoxide species appearing between δ −350 and −225 ppm and 2-coordinated Sn(II) alkoxide resonances reportedly fall between δ −100 to −175 ppm. Scheme 1 shows a graphical representation of the various ^{119}Sn shifts reported for Sn(OR)$_x$ compounds (note: the 4 coordinated Sn(IV) species Sn(NMe$_2$)$_4$ is observed at δ 0.0 ppm)[38] and those determined in this work. Obviously, the amide alkoxides do not exactly follow the Sn(OR)$_2$ trend and more work to verify the nuclearity is necessary. However, the clustering of the chemical shifts for **1–6** and the presence of one ^{119}Sn peak for each sample, implies these compounds all relatively pure in terms of the Sn precursor and they all adopt the same structure in solution.

Homoleptic

The aminolysis with the series of HOAr was again used to generate the homoleptic compounds following eqn (2). Upon addition of the HOAr to the pale yellow solution of [Sn(NMe$_2$)$_2$]$_2$ dissolved in toluene, the reaction mixture turned to an orange color, independent of the OAr used. After stirring for 12 h, X-ray quality crystals were isolated through slow evaporation of the volatile components. Based on the absence of the OH stretch at 3000 cm^{-1} and lack of NMe$_2$ stretches, FTIR data indicated the 'Sn(OAr)$_2$' species had been produced. Again the stretching modes of the *ν*(Sn–O) and *ν*(C–O)Sn were obfuscated by the OAr bends.[30–33] Additional information pertaining to the structure of the compound was necessary and crystal structures were obtained when possible.

The structures of the homoleptic products proved to be significantly varied from the dinuclear heteroleptic compounds. For **7** (Fig. 2) and **8**, polymeric structures were solved where each Sn(II) metal center adopted a tetra-coordination using μ-OAr ligands. Compounds **9**, **10** (Fig. 3), and **11** were found to adopt dinuclear arrangements with one terminal and two μ-OAr per metal center. Compound **11** (Fig. 4) also possesses one HNMe$_2$ bound to one of the Sn metal centers, which was verified by ^{1}H NMR and elemental analyses data (*vide infra*). Finally, a monomeric species was isolated with the most sterically hindered ligand (*i.e.*, DBP) identified as **12** (Fig. 5). The bent geometry forms an O–Sn–O angle of 89.0° due to the lone pair of electrons. A comparison of the metrical data for **7–12** were found to be self-consistent with longer Sn–(μ-OR) than Sn–(OR) distances. Comparable distances for this set of compounds and the heteroleptic (**1–6**) species were also found to be in agreement. Of the more than 500 previously reported, crystallographically characterized, homometallic Sn species, only five can be considered 'simple' aryloxide derivatives (all of which were monomeric) including (DBP,[39,40] DBP(Me)-4,[40] OC$_6$H$_2$(C$_6$H$_2$Me$_3$-2,4,6)$_2$,[41] OC$_6$H$_3$(C$_6$H$_3$(CH(CH$_3$)$_2$)$_2$-2,6),[42] OC$_6$H$_2$(CH$_2$NMe$_2$)$_3$-2,4,6[43]). The values obtained for **7–12** are in agreement when comparable angles and distances are analyzed.

Efforts were undertaken to determine if the bulk powders were in agreement with the single crystal structures obtained for the homoleptic species. The elemental analyses of the bulk powder

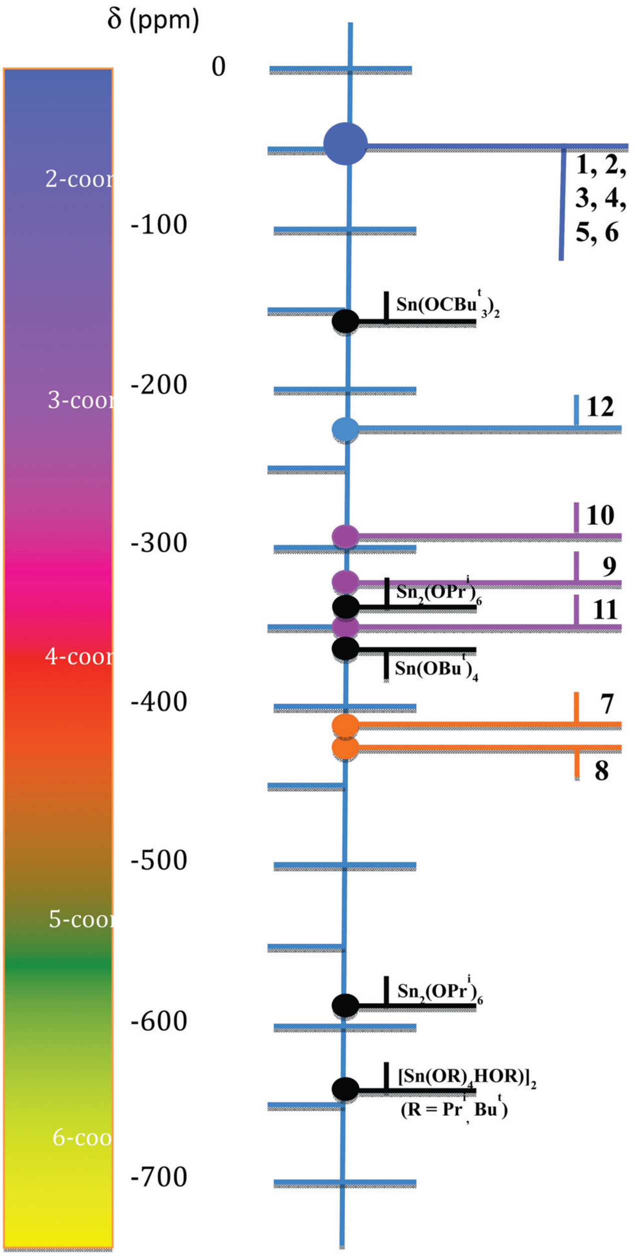

Scheme 1 ^{119}Sn chemical shift (major) of structurally characterized homoleptic tin alkoxide species: **black** – shifts from; ref. 38 **blue** – 2 coordinated heteroleptic; **pink** – 2 coordinated homoleptic, and **orange** 4-coordinated homoleptic.

were found to be in agreement with the single crystal structures of **8**, **10**, and **11**. For **7**, **9**, and **12** significant amounts of excess nitrogen was observed, which was assumed to be residual HNMe$_2$. The purity of the bulk powders was further investigated using solution state NMR. The ^{1}H and ^{13}C NMR spectrum of **7–11** revealed only one set of OAr ligand resonances for the respective compounds; again, some of the OAr peaks were obfuscated by the tol-d$_8$ resonances. The presence of only one set of ligand resonances implies that the solid state structures are disrupted in solution or the ligands are exchanging rapidly to generate one set of resonances. ^{119}Sn NMR data was collected to elucidate the solution behavior. The placement of these resonances (**7–12**) with the heteroleptic compounds (**1–6**) and literature Sn(OR)$_x$ are shown in Scheme 1. For **7**, **10**, and **12**, only one ^{119}Sn resonances was recorded indicates a relatively pure sample with simple solution behavior exists for these compounds. For **8**, **9**, and **11** two ^{119}Sn peaks were noted.

For the polymeric compounds **8**, the two ^{119}Sn shifts falls within the expected range noted for the 4-coordinated Sn(OR)$_x$. Since the previous analytical data indicates the bulk powder of **8** is consistent with the single crystal structure, the 3 : 1 ratio of ^{119}Sn shifts noted, **8** reflects an intermolecular process. This can be explained either by disruption of the polymer into unequivalent smaller chains or more likely inter-conversion of *cis-trans* of isomers around the lone pair of electrons on the Sn. For the dinuclear **9**, the two ^{119}Sn resonances (δ −315.7 to −323.0 ppm) were noted in a 3 : 97 ratio. The consistency of the shifts indicates that similar coordination environments around the Sn metal center must exist. Low temperature investigations could not be undertaken due to preferential precipitation. High temperature ^{119}Sn NMR spectra obtained on **9** revealed at 50 °C that the two room temperature peaks coalesced to a singlet at −329.1 ppm. Two potential explanations could account for this behavior: a *cis-trans* isomerization or a monomer–dimer equilibrium. The latter would yield two disparate chemical shifts representing the 2 and 3 coordinated Sn metal centers and therefore, inversion around the Sn metal center is assumed to be occurring yielding these two peaks. For **11**, two ^{119}Sn peaks were expected for the inequivalent 3- and 4- coordinated Sn metal centers found in the single crystal structure; however, while two peaks were observed (δ −121.6 and −340.5), the ratio was not the expected 1 : 1 but 9 : 91 instead. A number of complex equilibria or isomerizations can be used to explain the chemical shifts but the ratio implies an Sn-NMe$_2$ impurity is present. Additional work to further clarify the complex solution behavior of these homoleptic species is necessary.

Oxide compounds

From several attempts to crystallize the various compounds discussed above, a number of oxo- species were also isolated and crystallographically characterized. While rational routes to these compounds are being developed, the unit cell parameters and structural discussion are presented to assist in identifying the various products that can be generated in these reactions. Unit cell parameters are supplied in Table 1 for ease of identification with all structures and packing diagrams supplied in the ESI (Fig. S13–S15†). A brief description of each compound is supplied below.

Oxide structures of general formula Sn$_6$(μ$_3$-O)$_4$(μ$_3$-*o*PP)$_4$·solv (solv = py (**S1**) or H-*o*PP (**S2**)) were isolated from eqn (2) using H-*o*PP. The general arrangement consisted of six Sn atoms arranged in an octahedral geometry that are interconnected by alternating μ$_3$-O and μ$_3$-*o*PP ligands. This generates a series of interconnected ‘Sn(μ$_3$-O)(μ$_3$-*o*PP)Sn’ squares with a central void of 5.09 × 4.62 Å. The central core of this compound is consistent with that of other ‘Sn(O)$_x$(OR)$_y$’ compounds.[44–48] The different solvents for **S1** and **S2** are in the lattice. Another oxide (**S3**) was also formed from the attempt to generate the DIP derivative. The central core construct consists of a six membered ring of alternating Sn and O atoms from the DIP ligands. Each of the Sn atoms is bound to a μ_3-O atom, forming a corner missing cube shape. However, from each of these Sn atoms, a methoxide (OMe) ligand bridges to another Sn(4) atom. This results in the general construct of $\{[(\mu\text{-DIP})Sn]_3(\mu_3\text{-O})](\mu\text{-OMe})_3Sn\}$ (**S3**). For all of these compounds (**S1–S3**), the Sn atoms are in the +2 oxidation state, which makes formation of the oxide difficult to explain. Further, the production of the OMe in the **S3** compound is not fully understood and the reproduction of these compounds is not high. Therefore, these compounds are reported in Table 1 only to allow for identification of the desired complex. The distances in these compounds are similar to other oxide/alkoxides that we previously generated by hydrolysis of the alkoxide.[44–48]

Nanomaterial synthesis

With this newly developed family of hetero-(**1–6**) and homoleptic (**7–12**) derivatives available, attempts to synthesize SnO_x nanowires were undertaken. The results (*i.e.*, SEM, PXRD, etc) from these studies are presented for (a) SPPT followed by (b) ES methodologies.

(a) SPPT. The solvent system of oleylamine and octadecene was selected based on its propensity to form nanowires.[27] For the heteroleptic monosubstituted OAr derivatives (**1**, **2**, and **3**), large spheres on the order of one micron were observed with some nanosized (>20 nm) particles present. PXRD patterns for the materials generated from **1** indicated that only Sn^o (PDF 04-0673, tin) had been formed; however, for both **2** and **3** a mixture of phases [Sn^o, SnO (PDF 06-0395, romarchite), and SnO (PDF 04-1342, tin oxide)] in approximate ratios of 80 : 20 and 68 : 32, respectively. There are no indications from the TEM images (Fig. 6) of a different set of particles that would represent the oxides. The TEM images revealed that a variety of spherical sized particles and sizes were available. For compound **1** the particles ranged in size from 350–900 nm), for **2** from 150–1200 nm, and for **3** from 250–950 nm. There does not appear to be an influence from the changing sterics of the *ortho* substituents. For the di-substituted OAr species (**4–6**) mixed phases of Sn^o (PDF 04-0673) and SnO_x (PDF 06-0395) in approximate ratio of Sn^o : SnO of 86 : 14, 66 : 35, and 88 : 12, respectively, were isolated. The majority of the nanomaterials were Sn^o nanodots but both spheres and rods were present in TEM images (Fig. 6). The reduction of the Sn(II) to Sn^o in each of these systems is believed to be driven by the lone pair of electrons on the amine surfactant.[27] The size of the particles for the di-substituted OAr ligated compounds ranged for the various precursors **4** (20–180 nm); **5** (80–400 nm); **6** (40–200 nm) but, in comparison to **1–3** were smaller. This is attributed to the increased sterics around the metal center, which allows for increased solubility and protracted reactivity, resulting in the generation of simultaneous nucleation sites.

The homoleptic species (**7–12**) were also investigated and found to form similar spherical nanoparticles (Fig. 7), except for **9**. For the particles generated from **7**, **8**, **11**, and **12**, all were found to be spherical and of mixed phase [# (size, approximate ratio of Sn^o (04-0673):SnO(06-0395))]: **7** (50–300 nm, 80 : 20), **8** (irregular, 23 : 77), **11** (50–150 nm, 77 : 23), and **12** (50–450 nm, 77 : 23). For **9** (Fig. 7c), ∼100 nm wide polycrystalline rods of varied lengths leading to high aspect ratios (some >100) were noted in a ratio of Sn^o : romarchite (15 : 85). Compound **10** (Fig. 7d) generated spheres which had an approximate ratio of Sn^o : SnO (34 : 66) that ranged in size of 200–800 nm). In general, for **7–12**, these homoleptic species yielded similar size ranges for the resulting particles, indicating that the steric impact is much more limited for the homoleptic than the heteroleptic compounds. The higher degree of oxide to metal noted for these systems is most likely due to the presence of the two alkoxide ligands *versus* the amine in the heteroleptic species.

(b) ES. Since the SPPT products were mainly spherical, alternative routes were investigated to generate wires. Most of the routes that are available, such as the direct draw that produced high quality nanowires of SnO_2, are not a continuous process, which limit their utility in the production of LIB materials.[13] In contrast, ES[49–51] is a method that continuously produces fibers that can range in diameter from a few micrometers to 100 nanometers. This process works by applying a high electrical field to a drop of precursor solution pushed through a needle. The applied high electrical force overcomes the surface energy of the droplet and eventually forms a Taylor cone. The ejection of the solution forms a wire, which undergoes a whipping motion and collects on a metallic platform forming mats of fibers that possess a high surface area to mass ratio. Polymers are typically used to ensure a continuous linkage between drops and wires is made. We were interested in non-polymer based nanowires (*i.e.*, direct ES ceramic nanowires) to minimize post-processing and garner more control over the final materials produced. Unless alternating poles are used, ES generates a map of nanowires, which would still be of use in LIB applications. For this study, the ES investigations were undertaken in an argon filled glovebox. Upon application of the voltage, a purple plasma was formed and electrical discharges randomly occurred in the glovebox. It was determined that Ar has about 20% of the breakdown strength of N_2; therefore, all further experiments were conducted under an atmosphere of N_2.

For the ES studies, 0.66 M solutions in THF of the heteroleptic (**1–6**) precursors were employed and the SEM images of the various materials generated from these precursors are shown in Fig. 8. Except for **2**, the materials generated appear to be a mixture of electrospraying (*i.e.*, dots) *versus* ES (*i.e.*, wires) forming some unusual ‘tadpole’ shaped materials. This appears to be an effect where the Taylor cone has been initiated but the drop is dislodged prior to connecting to the next drop or the drop forms and stretches out to form a tail. The drops are several microns in size with nanometer wires forming (easily observed for both **1** and **4**). Wires with ‘balls’ strung along them have been observed previously for electrospun systems that lack chain entanglement and is often attributed to a high precursor concentration that may collapse the polymer coils and reduce chain entanglement.[51] Attempts to optimize the nanowires formed led to an exploration of different concentrations; however, the lower concentration solutions yielded electrosprayed materials and higher concentration solutions were too thick to be pumped. Therefore, the 0.66 M was maintained throughout this study.

For the majority of the homoleptic (**7–11**) species, attempts to ES these compounds under similar conditions noted for the heteroleptic series failed to form wires, instead electrospraying dots. This is not unexpected since the ability to chemically connect to

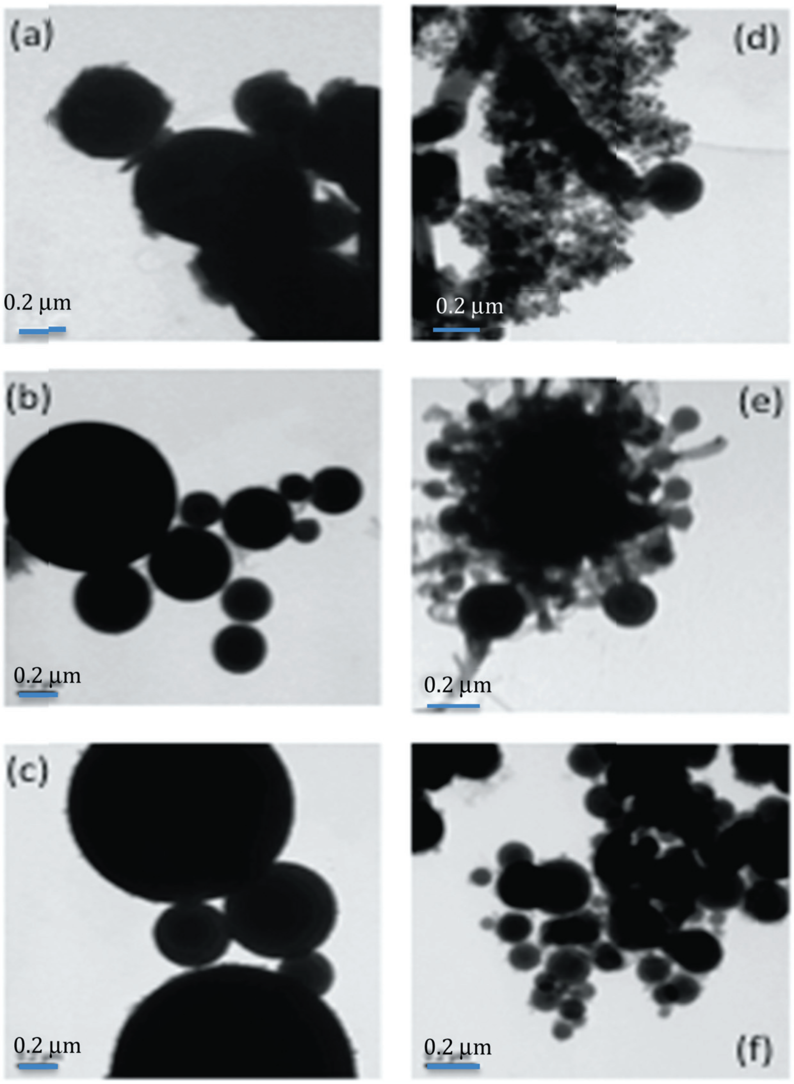

Fig. 6 TEM of nanomaterials generated from SPPT processing of: (a) **1**, (b) **2**, (c) **3**, (d) **4**, (e) **5**, and (f) **6**.

the next drop is limited with the di- and mono-nuclear compounds. The SEM images of these materials are shown in Fig. 9. Interesting, for the polymeric compound **7** (Fig. 9a) long nanowires with ~1 µm 'balls' strung along them at distant intervals were observed. These are the first reports of ceramic nanowires formed by ES methods that employs a single precursor dissolved in a solvent and does not require the aid of a polymer support or the addition of water;[52–62] however, it is of note that several other systems have utilized complex 'sols' that have successfully generated ceramic wires and tubes.[52–63] The system reported here employs only the dissolution of a single precursor in a solvent and the application of an electric field.

Due to small sample size generated by the ES process in this experiment, identification of the phase formed using PXRD analyses were not possible. Therefore, it became necessary to utilize other means to identify whether SnO_x or Sn^o had been formed. One effort that proved to be useful was cyclovoltammetry electrochemical (CVE) evaluations. By CVE methods, if SnO_x had been formed, then upon a reductive sweep in cyclic voltammetry, a Sn^{2+} to Sn^0 reduction peak at approximate −0.05 V *vs.* ref should be observed. If Sn^0 was present, no peak will be noted upon reduction but when doing an anodic sweep, an oxidation peak will be observed. Fig. 10 shows the CVE results for the four separate electrospun samples (2 h deposition time): (i) **1**, (ii) **1** for 8 h, (iii) **5**, and **7**. An additional blank of the graphite foil was used as a reference background for the voltammetry. All of the isothermal (25 °C) measurements made were performed at the same sweep rate (25 mV s^{-1}); therefore, any changes in the capacitance of the observed voltammetry have been attributed to changes in surface area due to deposition of material on the graphite foil. Neither the sample generate from **1** (2 h) nor from **5** yielded meaningful data, presumably due to the low levels of materials deposited.

For the samples generated from compound **1** (8 h) and **7**, sufficient material was present that allowed for electrochemical analysis. For **1** (8 h) electrospun materials, no peaks were noted for the first sweep. Subsequent sweeps showed similar peaks as those noted for the **7** materials. For the electrospun materials of **7**, no reduction peak on the first cathodic sweep, but a significant oxidation peak at approximately −50 mV (*vs.* ref) was observed,

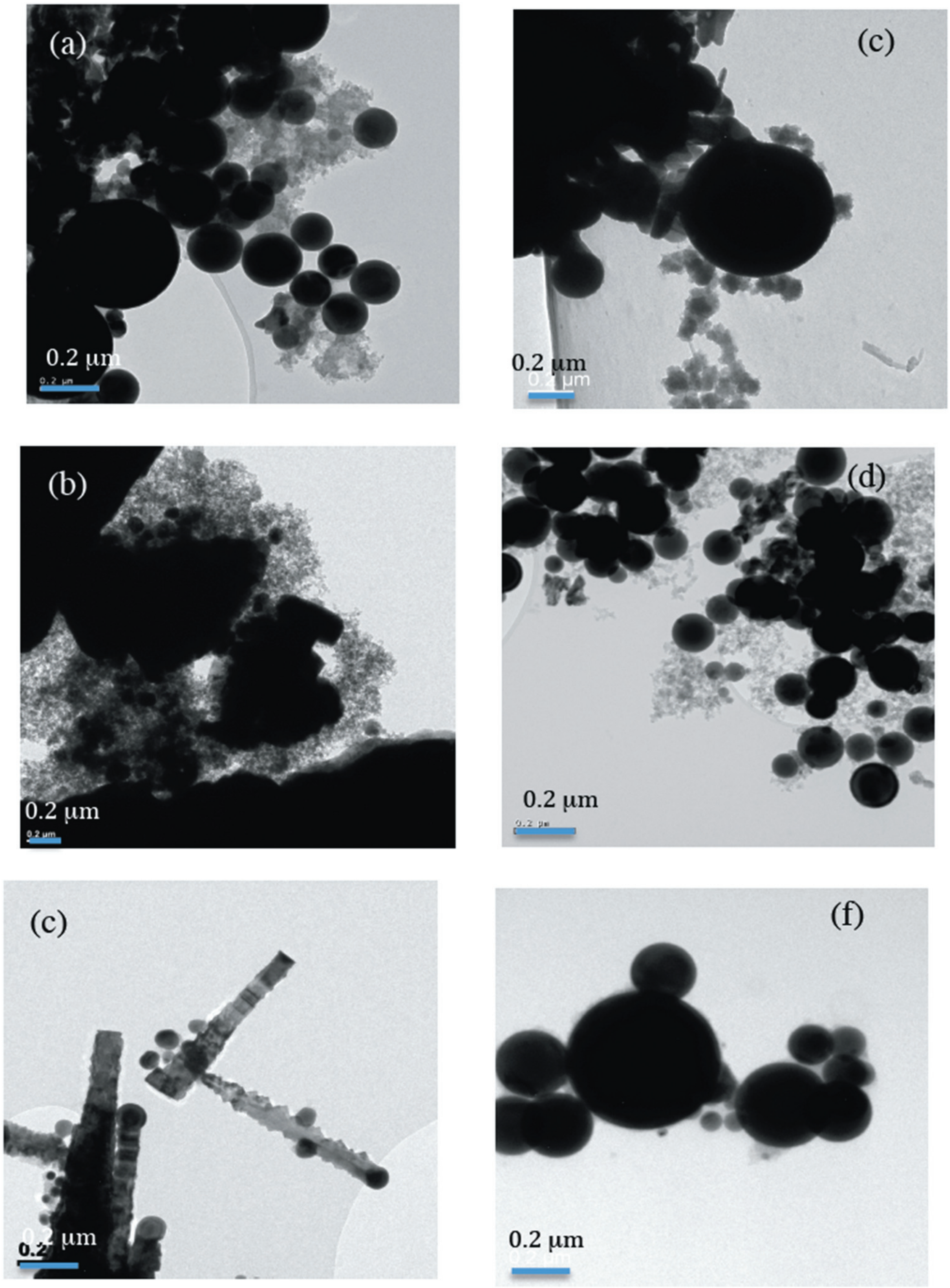

Fig. 7 TEM of nanomaterials generated from SPPT processing of: (a) **7**, (b) **8**, (c) **9**, (d) **10**, (e) **11**, and (f) **12**.

which is consistent with the potential of Sn^0 to Sn^{2+} oxidation. Subsequent cathodic sweeps on the same sample also showed a weak reductive peak around −130 mV, consistent with the re-reduction of oxidized Sn cations.

Since tin oxides are weakly soluble in CH_3CN, the gradual evolution of these peaks may be a result of the slow dissolution of the SnO_x followed by the electrochemical activation of the Sn material now present in the solution. Because of the low total oxidation current over a significant capacitive current on the samples, it is difficult to definitively identify the observed peaks as either the oxidation or reduction of the Sn that is present. However, the appearance of these peaks at the standard potentials for these reactions provides some argument that for **7**, a reduced state of Sn (*i.e.*, Sn^o) was deposited. This may also indicate that for the material deposited using **1** (8 h) was SnO_x instead of the reduced material, since there was no oxidation or reduction peak in the first sweep.

Summary and conclusion

A series of Sn(II) heteroleptic $[(OR)Sn(\mu\text{-}NMe_2)]_2$ and homoleptic $[Sn(OR)_2]_n$ derivatives were synthesized by aminolysis with the degree of substitution controlled by the stoichiometry of

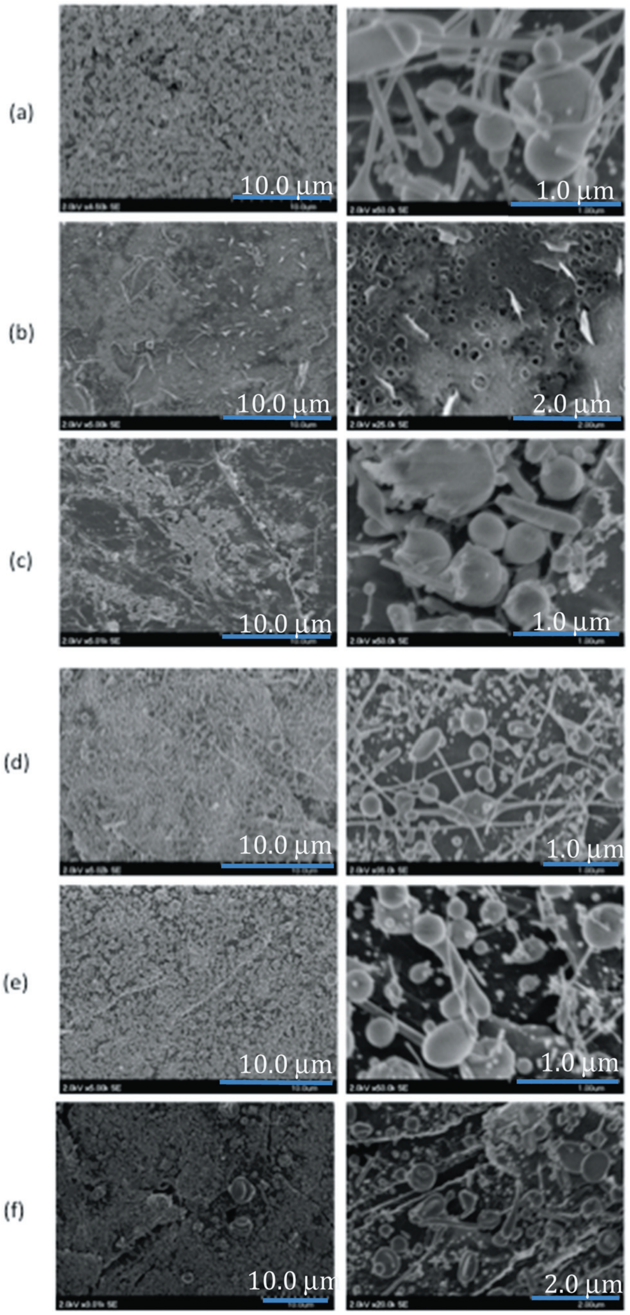

Fig. 8 SEM images of electrospun wires from (a) **1**, (b) **2**, (c) **3**, (d) **4**, (e) **5**, and (f) **6**.

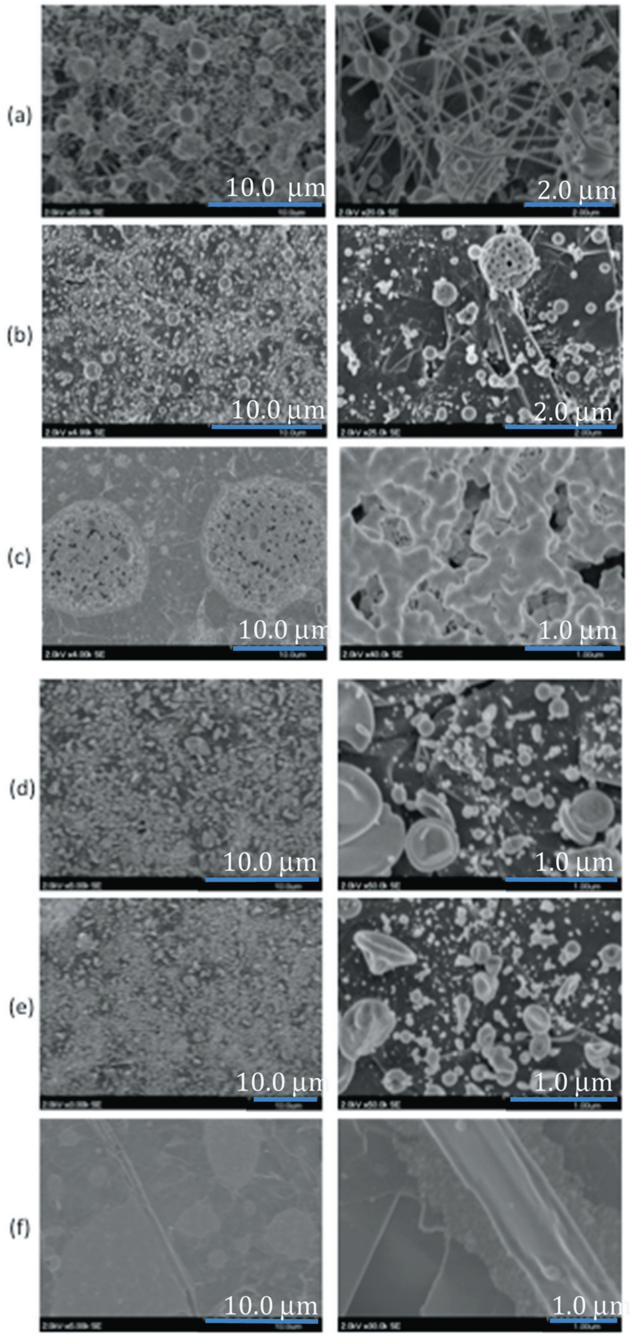

Fig. 9 SEM of images of electrospun wires from (a) **7**, (b) **8**, (c) **9**, (d) **10**, (e) **11**, and (f) **12**.

HOR modifier. The products isolated were predominately dinuclear (**1–6** and **9–11**) but polymeric (**7** and **8**) and mononuclear (**12**) species were isolated as well. The changes in the homoleptic series of compounds appear to be controlled by the steric bulk of the aryl substituent. These novel structurally diverse precursors were employed for production of nanowires. Under SPPT conditions, micron-sized spheres of mixed phased (Sn^o, romarchite, and SnO_x) materials were formed, where the heteroleptic species favor Sn^o nanoparticles and the homoleptic compounds favor the oxide phases. The variation in phases obtained was attributed to the free electrons of the amide moiety for the heteroleptic species. For **9**, rods were formed but were not regular enough to be of interest for battery applications. Attempts to electrospin the heteroleptic compounds yielded 'tadpole' shaped materials, whereas the homoleptic species merely electrosprayed. The one exception was **7**, which formed nanowires with micron-sized 'balls' strung along them. Efforts to understand the impact of the various ligand sets on the different material's morphologies are underway.

However, it is of note that the resultant ceramic nanowires were generated using a precursor dissolved in a solvent, which contrasts to previous efforts that necessitated the use of a polymer, water, or complex sol synthesis. More work to improve

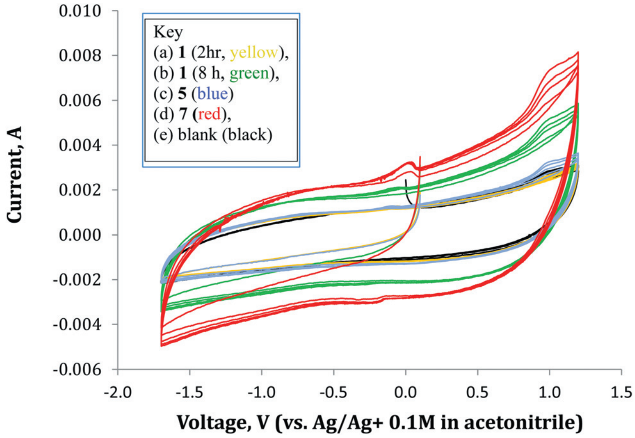

Fig. 10 Cyclic voltammograms of electrospun wires (2 h) from precursor (a) **1** (yellow), (b) **1** (8 h, green), (c) **5** (blue) (d) **7** (red), (e) blank (black).

the morphological properties of these nanowires and extending this process to other polymer free ceramic materials is underway. Preliminary electrochemical studies indicated that compound **7** may have formed Sn^o nanowires during deposition; whereas the material generated from **1** (8 h) was preliminarily identified as SnO_x. Additional work employing CVE methods on the precursors are underway to elucidate the mechanism of formation of these materials, since (under the conditions used in this work) ES utilizes an electrical field to decompose the precursor and does not undergo standard hydrolysis condensations.[2,25,26] Further work on molecular design or processing conditions to control the phases formed along with development of new methods for testing the generated LIB anode materials is underway.

Acknowledgements

The authors would like to thank Dr M. A. Rodriguez (SNL) for assistance in the PXRD analyses, Dr T. M. Alam for assistance with NMR analyses, and Prof. Kemp (UNM) for the use of the Bruker X-ray diffractometer purchased *via* the National Science Foundation CRIF:MU award to the University of New Mexico (CHE04-43580). This work was supported by the National Institute for NanoEngineering (NINE) and the Laboratory Directed Research and Development (LDRD) programs at Sandia National Laboratories. Sandia National Laboratories is a multi-program laboratory managed and operated by Sandia Corporation, a wholly owned subsidiary of Lockheed Martin Corporation, for the U.S. Department of Energy's National Nuclear Security Administration under contract DE-AC04-94AL85000.

References

1 P. F. Gao and J. Yang, *Prog. Chem.*, 2011, **23**, 264–274.
2 V. G. Kessler and G. A. Seisenbaeva, *Sol–Gel Methods for Materials Processing*, Springer, Berlin, 2008.
3 C. K. Chan, H. Peng, G. Liu, K. McIlwrath, X. F. Zhang, R. A. Huggins and Y. Cui, *Nat. Technol.*, 2008, **3**, 31–35.
4 W.-M. Zhang, J.-S. Hu, Y.-G. Guo, S.-F. Zheng, L.-S. Zhong, W.-G. Song and L.-J. Wan, *Adv. Mater.*, 2008, **20**, 1160–1165.
5 O. Mao, R. A. Dunlap and J. R. Dahn, *J. Electrochem. Soc.*, 1999, **146**, 405–413.
6 C. Wang, A. J. Appleby and F. E. Little, *J. Power Sources*, 2001, **93**, 174–185.
7 G. XIa, N. Li, D. Li, R. Liu, N. Xiao and D. Tian, *Mater. Lett.*, 2011, **65**, 3377–3379.
8 Y. Wang and J. Y. Lee, *J. Phys. Chem. B*, 2004, **108**, 17832–17837.
9 Y.-D. Ko, J.-G. Kang, J.-G. Park, S. Lee and D.-W. Kim, *Nanotechnology*, 2009, **20**, 455701:455701–455706.
10 M.-S. Park, G.-X. Wang, Y.-M. Kang, D. Wexler, S.-X. Dou and H.-K. Liu, *Angew. Chem., Int. Ed.*, 2007, **46**, 750–753.
11 H. Kim and J. Cho, *J. Mater. Chem.*, 2008, **18**, 771–775.
12 W. Wang, C. Xu, G. Wang, Y. Liu and C. Zheng, *J. Appl. Phys.*, 2002, **92**, 2740–2742.
13 T. Tatte, M. Hussainov, M. Paalo, M. Part, R. Talviste, V. Kiisk, H. Mandar, K. Pohako, T. Pehk, K. Reivelt, M. G. Natali, J. A. Lohmus and U. Maeorg, *Sci. Technol. Adv. Mater.*, 2011, **12**, 034412.
14 B. A. Hernandez-Sanchez, T. J. Boyle, H. D. I. Pratt, M. A. Rodriguez, L. N. Brewer and D. R. Dunphy, *Chem. Mater.*, 2008, **20**, 6643–6656.
15 T. J. Boyle, S. D. Bunge, N. L. Andrews, L. E. Matzen, K. Sieg, M. A. Rodriguez and T. J. Headley, *Chem. Mater.*, 2004, **16**, 3279–3288.
16 H. Gerung, T. J. Boyle, L. J. Tribby, S. D. Bunge, C. J. Brinker and S. M. Han, *J. Am. Chem. Soc.*, 2006, **128**, 5244–5250.
17 Y. T. Wong, N. B. Wong and L. Shi, *J. Mater. Sci.*, 2003, **38**, 973–977.
18 M. C. Cabajo, C. Lopez, A. Gomez, E. Enciso and M. J. Torralvo, *J. Mater. Chem.*, 2003, **13**, 2311–2316.
19 C. Isobe, K. Hironaka and S. Hishikawa, *Adv. Mater. Opt. Electron.*, 2000, **10**, 183–191.
20 B. Malic, M. Kosec, I. Arcon, A. Kodre, S. Hiboux and P. Muralt, *Integr. Ferroelectr.*, 2000, **30**, 81–89.
21 M. Kosec and B. Malic, *J. Phys. IV*, 1998, **8**, 17–26.
22 J. Blanchard, M. In, B. Schaudel and C. Snachez, *Eur. J. Inorg. Chem.*, 1998, 1115–1127.
23 J. S. Liu, T. W. Xu, M. Gong and Y. X. Fu, *J. Membr. Sci.*, 2005, **260**, 26–36.
24 C. Mui and C. B. Musgrave, *J. Phys. Chem. B*, 2004, **108**, 15150–15164.
25 V. G. Kessler, G. I. Spijksma, G. A. Seisenbaeva, S. Hakansson, D. H. S. Blank and H. J. M. Bouwmeester, *J. Sol-Gel Sci. Technol.*, 2006, **40**, 163–179.
26 N. Y. Turova, *Russ. Chem. Rev.*, 2004, **73**, 1041–1064.
27 T. J. Boyle, T. M. Alam, M. A. Rodriguez and C. A. Zechmann, *Inorg. Chem.*, 2002, **41**, 2574–2582.
28 M. M. Olmstead and P. P. Power, *Inorg. Chem.*, 1984, **23**, 413–415.
29 E. Weiss, H. Alsdorf and H. Huhr, *Angew. Chem.*, 1967, **79**, 816.
30 D. C. Bradley, R. C. Mehrotra and D. P. Gaul, *Metal Alkoxides*, Academic Press, New York, 1978.
31 L. PaQuette and W. Farley, *J. Org. Chem.*, 1967, **32**, 2718–2719.
32 A. Volod'kin and G. Zaikov, *Chem. Chem. Technol.*, 2010, **4**, 179–184.
33 J. B. Hendrickson, D. J. Cram and G. S. Hammond, *Organic Chemistry*, McGraw-Hill Book Company, New York, 3rd edn, 1970.
34 G. D. Smith, P. E. Fanwick and I. P. Rothwell, *Inorg. Chem.*, 1990, **29**, 3221–3226.
35 M. J. McGeary, K. Folting and K. G. Caulton, *Inorg. Chem.*, 1989, **28**, 4051–4053.
36 V. N. Khrustalev, I. A. Portnyagin, N. N. Zemlyansky, I. V. Borisova, M. S. Nechaev, Y. A. Ustynyuk, M. Y. Antipin and V. Lunin, *J. Organomet. Chem.*, 2005, **690**, 1172–1177.
37 N. Nimitsiriwat, V. C. Gibson, E. L. Marshall and M. R. Elsegood, *Dalton Trans.*, 2009, 3710–3715.
38 D. J. Teff, C. D. Minear, D. V. Baxter and K. G. Caulton, *Inorg. Chem.*, 1998, **37**, 2547–2553.
39 D. M. Barnhart, D. L. Clark and J. G. Watkin, *Acta Crystallogr., Sect. C: Cryst. Struct. Commun.*, 1994, **50**, 702–704.
40 B. Cetinkaya, I. Gumrukcu, M. F. Lappert, J. L. Atwood, R. D. Rogers and M. J. Zaworotko, *J. Am. Chem. Soc.*, 1980, **102**, 2088–2089.
41 D. A. Dickie, I. S. Macintosh, D. D. Ino, Q. He, O. A. Labeodan, M. C. Jennings, G. Schatte, C. J. Walsby and J. A. C. Clyburne, *Can. J. Chem.*, 2008, **86**, 20–31.
42 C. Stanciu, A. F. Richards, M. Stender, M. M. Olmstead and P. P. Power, *Polyhedron*, 2006, **25**, 477–483.
43 N. N. Zemlyansky, I. V. Borisova, M. G. Kuznetsova, V. N. Khrustalev, Y. A. Ustynyuk, M. S. Nechaev, V. V. Lunin, J. Barrau and G. Rima, *Organometallics*, 2003, **22**, 1675–1681.
44 T. J. Boyle, T. M. Alam, M. A. Rodriguez and C. A. Zechmann, *Inorg. Chem.*, 2002, **41**, 2574–2582.

45 R. A. Howie and W. Moser, *Nature*, 1968, **219**, 372–373.
46 Y. Sasaki and N. Miyazawa, *Kinki Daigaku Rikogakubu Kenkyu Hokoku*, 1992, **28**, 237.
47 L. R. Sita, R. Xi, G. P. A. Yap, L. M. Liable-Sands and A. L. Rheingold, *J. Am. Chem. Soc.*, 1997, **119**, 756–760.
48 P. G. Harrison, B. J. Haylett and T. J. King, *J. Chem. Soc., Chem. Commun.*, 1978, 112–113.
49 M. J. Laudenslager, R. Schleffler and W. M. Sigmund, *Pure Appl. Chem.*, 2010, **82**, 2137–2156.
50 M. J. Laudenslager and W. M. Sigmund, *Am. Ceram. Soc. Bull.*, 2011, **90**, 22–26.
51 W. M. Sigmund, J. Yuh, H. Park, V. Maneeratana, G. Pyrgiotakis, A. Daga, J. Taylor and J. C. Nino, *J. Am. Ceram. Soc.*, 2006, **89**, 395–407.
52 W. K. Son, D. Cho and W. H. Park, *Nanotechnology*, 2006, **17**, 439–443.
53 H. Dai, J. Gong, H. Kim and D. Lee, *Nanotechnology*, 2002, **13**, 674–677.
54 D. Li and Y. Xia, *Nano Lett.*, 2003, **3**, 555–560.
55 B. Ding, C. K. Kim, H. Y. Kim, M. K. Seo and S. J. Park, *Fibers Polym.*, 2004, **5**, 105–109.
56 S. Madhugiri, B. Sun, P. G. Smirniotis, J. P. G. Ferraris and K. J. J. Balkus, *Microporous Mesoporous Mater.*, 2004, **69**, 77–83.
57 S. Lee, C. Tekmen and W. M. Sigmund, *Mater. Sci. Eng., A*, 2005, **398**, 77–81.
58 B. Ding, H. Kim, C. K. Kim, M. Khil and S. Park, *Nanotechnology*, 2003, **14**, 532–537.
59 G. Larsen, R. Velarde-Ortiz, K. Minchow, A. Barrero and I. G. Loscertales, *J. Am. Chem. Soc.*, 2003, **125**, 1154–1155.
60 C. Shao, H. Kim, J. Gong, B. Ding, D. Lee and S. Park, *Mater. Lett.*, 2003, **57**, 1579–1584.
61 S. S. Choi, S. G. Lee, S. S. Im, S. H. Kim and Y. L. Joo, *J. Mater. Sci. Lett.*, 2003, **22**, 891–893.
62 E. Riedel, S. Horvath-Bordon, S. B. Nahar and E. Kroke, *Adv. Ceram. Comp.*, 2003, **247**, 121–128.
63 V. Maneeratana and W. M. Sigmund, *Chem. Eng. J.*, 2008, **137**, 137–143.